

## RESEARCH ARTICLE

## iASPP is a novel autophagy inhibitor in keratinocytes

Anissa Chikh<sup>1</sup>, Paolo Sanzà<sup>1</sup>, Claudio Raimondi<sup>2,\*</sup>, Olufolake Akinduro<sup>1</sup>, Gary Warnes<sup>3</sup>, Giovanna Chiorino<sup>4</sup>, Carolyn Byrne<sup>1</sup>, Catherine A. Harwood<sup>1</sup> and Daniele Bergamaschi<sup>1,‡</sup>

## ABSTRACT

The protein iASPP (encoded by *PPP1R13L*) is an evolutionarily conserved p53 inhibitor, the expression of which is often upregulated in human cancers. We have recently shown that iASPP is a crucial regulator of epidermal homeostasis. Here, we report that iASPP also acts as autophagy inhibitor in keratinocytes. Our data show that depletion of iASPP protects keratinocytes from apoptosis by modulating the expression of Noxa (also known as PMAIP1). In our model, iASPP expression can affect the fission-fusion cycle, mass and shape of mitochondria. iASPP-silenced keratinocytes display disorganization of cytosolic compartments and increased metabolic stress caused by deregulation of mTORC1 signaling. Moreover, increased levels of lipidated LC3 protein confirmed the activation of autophagy in iASPP-depleted cells. We have identified a novel mechanism modulating autophagy in keratinocytes that relies upon iASPP expression specifically reducing the interaction of Atg5–Atg12 with Atg16L1, an interaction that is essential for autophagosome formation or maturation. Using organotypic culture, we further explored the link between autophagy and differentiation, and we showed that impairing autophagy affects epidermal terminal differentiation. Our data provide an alternative mechanism to explain how epithelial integrity is maintained against environmental stressors and might also improve the understanding of the etiology of skin diseases that are characterized by defects in differentiation and DNA damage responses.

**KEY WORDS:** IASPP, Apoptosis, Autophagy, Mitochondria, Epidermis, Keratinocytes

## INTRODUCTION

The epidermis is a continuously renewing multilayered epithelium of the skin, in which all steps of keratinocyte differentiation occur sequentially, with each process characterized by the expression of specific markers (Fuchs, 1990; Watt, 1989). The pathways leading to terminal differentiation involve the removal of cell organelles, mediated in part by the activation of lysosomal enzymes, which are therefore essential for maintaining homeostasis of the skin (Candi et al., 2005).

The ASPP proteins are a group of p53 co-activators (Trigiante and Lu, 2006). The apoptotic function of p53 is potentiated by ASPP1 and ASPP2, whereas a third family member, iASPP, negatively modulates it. iASPP (encoded by *PPP1R13L*) is evolutionarily conserved from worm to human, and its expression is frequently upregulated in human cancers (Bergamaschi et al., 2003; Bergamaschi et al., 2006; Cao et al., 2013; Chen et al., 2010; Kabeya et al., 2000; Liu et al., 2009; Liu et al., 2012; Lu et al., 2010; Mantovani et al., 2007; Sæbø et al., 2006; Zhang et al., 2005). iASPP is expressed predominantly in epithelial cells, in the skin, testis, heart and stomach (Herron et al., 2005). Mutations in *PPP1R13L* cause abnormalities of the heart, skin and hair, in both mice and cattle (Herron et al., 2005; Simpson et al., 2009; Toonen et al., 2012). Mice of the *wa3* phenotype (which carry a 14-bp deletion in *Ppp1r13l*, resulting in a loss of the SH3-domain at the C-terminal end of the protein) display wavy hair and open eyelids at birth (EOB), and they develop a rapidly progressive cardiomyopathy (Herron et al., 2005). More recently, *woe2* mice have been found to show a novel spontaneous *PPP1R13L* mutation, resulting in the loss of 223 amino acids from the C-terminal end of the protein. In addition to the EOB, wavy fur and cardiac phenotypes that were characterized previously, *woe2* mice also exhibit defects in the development of the anterior segment of the eye and the absence of meibomian glands (Toonen et al., 2012). The cattle that harbor a frame-shift mutation in bovine *PPP1R13L* also exhibit cardiomyopathy and a woolly hair coat (Simpson et al., 2009).

Two recent molecular studies have shown that iASPP is expressed from early stages of development through to adult epidermis, where it partially colocalizes with p63 (encoded by *TP63*) (Chikh et al., 2011; Notari et al., 2011). Moreover, a novel autoregulatory feedback mechanism functioning between iASPP and p63 has been identified in keratinocytes, whereby p63 modulates iASPP, and iASPP directly represses two previously unreported miRNAs, miR-720 and miR-574-3p, which, in turn, control the expression of the  $\Delta$ Np63 isoform by preventing its translation. iASPP and p63 are therefore linked in the maintenance of epidermal homeostasis by regulating genes that are essential for cell adhesion, differentiation and proliferation in the stratified epithelia.

Several reports have recently described the autophagy process occurring in monolayer cultures of keratinocytes (Aymard et al., 2011; Chatterjea et al., 2011; Deruy et al., 2010; Gosselin et al., 2009; Lee et al., 2011; Silva et al., 2010; Tong et al., 2012; Wang and Levine, 2011; Zhao et al., 2013; Zhou and Munger, 2009). Autophagy is a highly conserved proteolytic mechanism that maintains the homeostasis of the cell by degrading organelles and cytoplasmic material. The sequestration of cytoplasmic components in vesicles (autophagosomes) and their delivery to lysosomes is controlled by autophagy-related genes (Atgs). Two main ubiquitin-like conjugation systems that are essential for the

<sup>1</sup>Centre for Cutaneous Research, Blizard Institute, Barts and The London School of Medicine and Dentistry, Queen Mary University of London, London E1 2AT, UK.

<sup>2</sup>Centre for Diabetes, Blizard Institute, Barts and The London School of Medicine and Dentistry, Queen Mary University of London, London E1 2AT, UK. <sup>3</sup>Flow Cytometry Core Facility, Blizard Institute, Barts and The London School of Medicine and Dentistry, Queen Mary University of London, London E1 2AT, UK.

<sup>4</sup>Cancer Genomic Laboratory, Edo ed Elvo Tempia Foundation, 13900 Biella, Italy. \*Present address: UCL Institute of Ophthalmology, University College London, London EC1V 9EL, UK.

<sup>‡</sup>Author for correspondence (d.bergamaschi@qmul.ac.uk)

formation of autophagosomes are the Atg5–Atg12 complex and the microtubule-associated protein light chain 3 (LC3) (Mizushima et al., 2011). Metabolic stress induces cells to undergo autophagy, which could lead to differentiation, such as in erythropoiesis (Griffiths et al., 2012) or adipogenesis (Baerga et al., 2009). Recent evidence linking autophagy to apoptosis highlights the involvement of Noxa in the process (Tormo et al., 2009). In keratinocytes, UV-B irradiation requires Noxa activation in order to induce apoptosis (Naik et al., 2007), and this can be p53-dependent or p53-independent (Nys et al., 2010; Villunger et al., 2003). Autophagy is a metabolic process of central importance in cell fate decisions, as it can either protect cells by preventing apoptosis or can result in cell death (Lum et al., 2005; Ravikumar and Rubinsztein, 2006). In our previous report, we demonstrated that iASPP is crucial for the fine-tuning of homeostasis in the basal layer of the epidermis (Chikh et al., 2011). Keratinocytes silenced for iASPP generated a markedly thicker epidermis, demonstrating that depletion of iASPP promotes and accelerates differentiation while simultaneously inhibiting the proliferation process in the stratified epidermis of the skin. The role of autophagy in the epidermis is still poorly understood. A couple of very recent reports have shown that, in mouse models, blocking the Atg5- and Atg7-dependent autophagy pathway has no functional consequence for skin development, with formation of an intact skin barrier (Rossiter et al., 2013; Sukseree et al., 2013). This raises the question of whether all the autophagy streams occurring in the epidermis can be impaired by simply inhibiting one of the main signaling pathways involved in the formation of autophagosomes. Recent reports from Shimizu's laboratory clearly demonstrate the existence of at least one alternative Atg5/Atg7-independent macroautophagy pathway in mammalian cells (Nishida et al., 2009; Shimizu et al., 2010). Unlike canonical macroautophagy, the observed Atg5/Atg7-independent autophagy pathway forms Rab9-positive double-membraned vesicles derived from the trans-Golgi network and late endosomes. This process is dependent on beclin-1, and occurs independently of Atg5 and LC3. More recently, another alternative autophagy pathway has been reported, involving a ubiquitin enzyme, Uba1, which is required for autophagy and reduction of cell size in *Drosophila* in the absence of Atg7 and Atg3 (Chang et al., 2013). Here, we unveil a novel function of iASPP, the expression of which is important for modulating the autophagy metabolic process and for maintaining mitochondrial integrity. We report that decreased iASPP expression could prevent the apoptotic signaling in keratinocytes through Noxa and trigger autophagy by depression of the Atg5–Atg12–Atg16L1 complex, promoting autophagosome maturation. Finally, we explore the molecular links between autophagy and keratinocyte differentiation controlled by iASPP.

## RESULTS

### iASPP depletion protects cells from apoptosis by modulating Noxa expression

To establish the role of iASPP in the DNA damage response, keratinocytes from which iASPP was depleted using short hairpin (sh)RNA were exposed to different apoptotic inducers, including staurosporine and UV-B radiation. Assessment of annexin-V staining at 24 h using flow cytometry revealed that control cultures showed increased apoptosis upon treatment, whereas keratinocytes depleted of iASPP displayed greater resistance to apoptosis (Fig. 1A). To understand the molecular mechanisms

underlying the resistance to apoptosis demonstrated by iASPP-depleted keratinocytes, we evaluated the expression levels of *PMAIP1*, the gene encoding Noxa, which we found to be downregulated in our previously published microarray analysis of iASPP-depleted cells (Chikh et al., 2011) (Fig. 1B). Upon UV-B exposure, Noxa is activated and is essential for the induction of apoptosis in keratinocytes. The downregulation of *PMAIP1* mRNA levels and Noxa protein levels was confirmed in several types of sh-iASPP keratinocytes (Fig. 1C). Further analysis of some of the other Bcl-2 protein family members revealed that, apart from cell-type specific downregulation of Bak protein, a consistent downregulation of anti-apoptotic Mcl-1 protein also occurred (Fig. 1D; supplementary material Fig. S1A). Rescue experiments showed that re-expression of either exogenous Noxa or Bak was sufficient to restore the apoptotic sensitivity of iASPP-silenced keratinocytes (Fig. 1E; supplementary material Fig. S1B). Moreover, specific siRNA-mediated downregulation of Noxa in primary keratinocytes failed to modulate iASPP protein expression, confirming the notion that Noxa is one of the main driving forces of the cell death response in keratinocytes, directly affecting the expression of pro-apoptotic targets, such as Puma (also known as BBC3), pro-caspase 8 and pro-caspase 9 (Fig. 1F). Silencing of Noxa in the presence of iASPP triggered a potential compensatory effect by upregulating the expression of Bak protein (Fig. 1F), confirming the activation of a different signaling pathway.

### iASPP expression is crucial for mitochondrial integrity

Given the effect of iASPP in modulating Noxa expression, we decided to further explore the expression of other key regulators of mitochondrial membrane integrity. To investigate the role of iASPP in mitochondrial homeostasis, keratinocytes were fractionated into cytoplasmic and mitochondrial intracellular components. Western blot analysis revealed that a fraction of cytoplasmic iASPP is expressed within the mitochondria (Fig. 2A). Furthermore, by using confocal microscopy, we assessed the effect of iASPP knockdown on mitochondrial morphology in two different keratinocyte cell lines (Fig. 2B; supplementary material Fig. S1C). The dynamic balance between fission and fusion controls the maintenance of functional mitochondria. Control cells displayed tubular and branched organelles, whereas the keratinocytes depleted for iASPP had an increased number of small mitochondrial fragments derived from mitochondrial fission in the absence of fusion. We confirmed these observations by monitoring the classic fission and fusion markers by western blot analysis in two different keratinocyte cell lines (Fig. 2C). Mitofusin (MFN)1 and MFN2, key components of the mitochondrial fusion machinery, were drastically depleted in the cells silenced for iASPP, whereas the expression of other factors required for mitochondrial fusion, such as OPA1, was unaffected. Likewise, decreased expression of both mitofusins was confirmed at the transcriptional level in iASPP-depleted cells (Fig. 2D), hinting at a possible regulation of mitofusin transcription by iASPP. However, the expression of phosphorylated (phospho)-DRP1 (encoded by *DNM1L*), an essential regulator of the fission machinery in mitochondria, was upregulated in the same cells (whereas the expression of total DRP1 was unaffected) (Fig. 2C), indicating a shift towards fission with the consequent production of mitochondrial fragments. This phenotype was a consequence of iASPP depletion and was unaffected by Noxa expression, because Noxa depletion did not alter the expression of mitochondrial fusion markers in the same

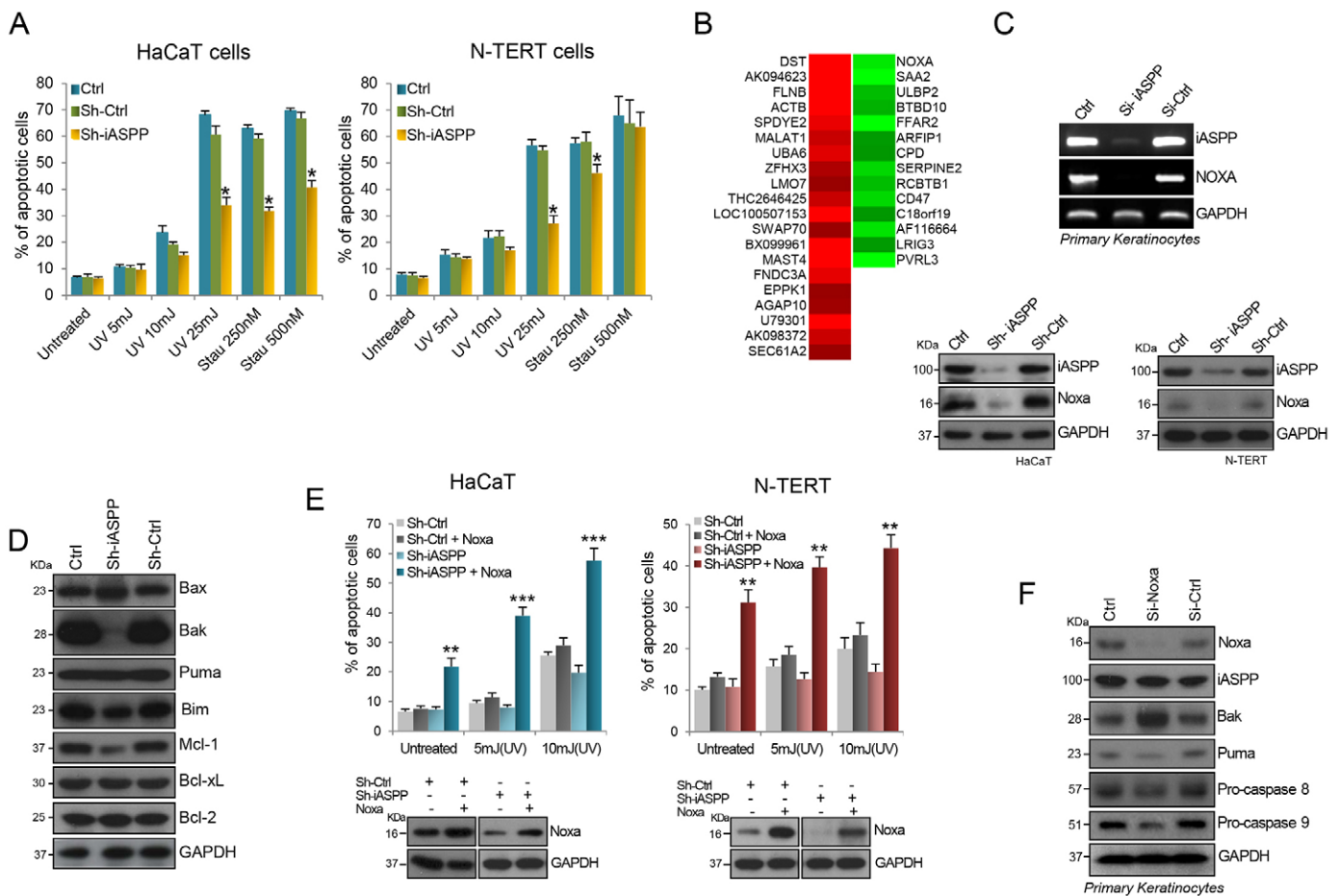


**Fig. 1. iASPP depletion protects cells from apoptosis by modulating Noxa expression.** (A) Apoptosis assay in HaCaT and N-TERT cells treated with UV-B and staurosporine at increasing doses. Cell death (% apoptotic cells) was quantified by using flow cytometric analysis of annexin-V- and propidium-iodide-positive populations. Ctrl, control. Results represent the mean  $\pm$  s.e.m. (three independent experiments performed in duplicate); \* $P$  < 0.05 (two-tailed Student's  $t$ -test). (B) Comparative analysis of genes modulated by iASPP silencing (sh-iASPP versus sh-Ctrl condition) using the Agilent platform. A red-to-green gradient was used to indicate, for each gene, levels of up- or down-regulation, respectively, expressed as log<sub>2</sub> (ratio) values. (C) Validation of Noxa downregulation from the array analysis by RT-PCR on primary keratinocytes depleted for iASPP (upper panel) and by western blot analysis (lower panels) performed on HaCaT and N-TERT sh-iASPP cells. (D) Western blot analysis of the effects of iASPP knockdown on members of the Bcl-2 family in HaCaT cells. (E) Apoptosis assay in HaCaT (sh-Ctrl and sh-iASPP) and N-TERT (sh-Ctrl and sh-iASPP) cells exposed to increasing UV-B doses with or without rescue of Noxa expression by transfection. Cell death (% apoptotic cells) was measured by flow cytometric analysis of annexin-V- and DAPI-positive populations. Results represent the mean  $\pm$  s.e.m. (three independent experiments performed in duplicate); \*\* $P$  < 0.01; \*\*\* $P$  < 0.001 (two-tailed Student's  $t$ -test). Lower panel, western blot analysis confirms overexpression of Noxa in the sh-iASPP HaCaT and N-TERT cells versus sh-Ctrl cells. (F) Western blot analysis of target proteins affected by Noxa depletion in primary keratinocytes. For C–F, GAPDH was used as a loading control.

manner. Noxa silencing instead decreased the levels of phospho-DRP1, perhaps compromising the mitochondrial fission process (supplementary material Fig. S1D). Moreover, depletion of either Bak or Mcl-1 in the same cellular system did not cause similar changes in the expression of mitochondrial fission and fusion markers when compared with depletion of iASPP (supplementary material Fig. S1E,F). Interestingly, keratinocytes knocked down for iASPP also showed an increased mitochondrial mass, confirmed by upregulation of the expression of Tomm20 (an outer mitochondrial membrane marker) (Fig. 2E). Furthermore, the mitochondrial membrane potential ( $\Delta\psi_m$ ) was measured in cells knocked down for iASPP versus control cells. We observed hyperpolarization of the mitochondria in iASPP-depleted cells, comparable to that displayed by differentiated cells (Fig. 2F; supplementary material Fig. S2A–C). Hyperpolarization of the mitochondrial membrane normally prevents the release of apoptotic factors. Therefore, these data further confirm the

cytoprotective effect of iASPP silencing in the keratinocyte lineage. Mitochondrial impairment was further evaluated by measuring the level of reactive oxygen species (ROS) using MitoSOX staining coupled with flow cytometry in control versus iASPP-silenced keratinocytes. In our cell system, ROS levels were increased in iASPP-silenced differentiated live cells compared with the levels in controls, hinting at a relationship between differentiation and the absence of apoptosis (Fig. 2G; supplementary material Fig. S2A).

#### iASPP depletion changes the cytosolic architecture and induces metabolic stress

Analysis of the biological processes affected by iASPP silencing from the gene expression profiles determined by microarray (shown in Fig. 1B) revealed that iASPP depletion mainly affects the development of cellular structures but also drastically influences cellular metabolic processes (Fig. 3A).

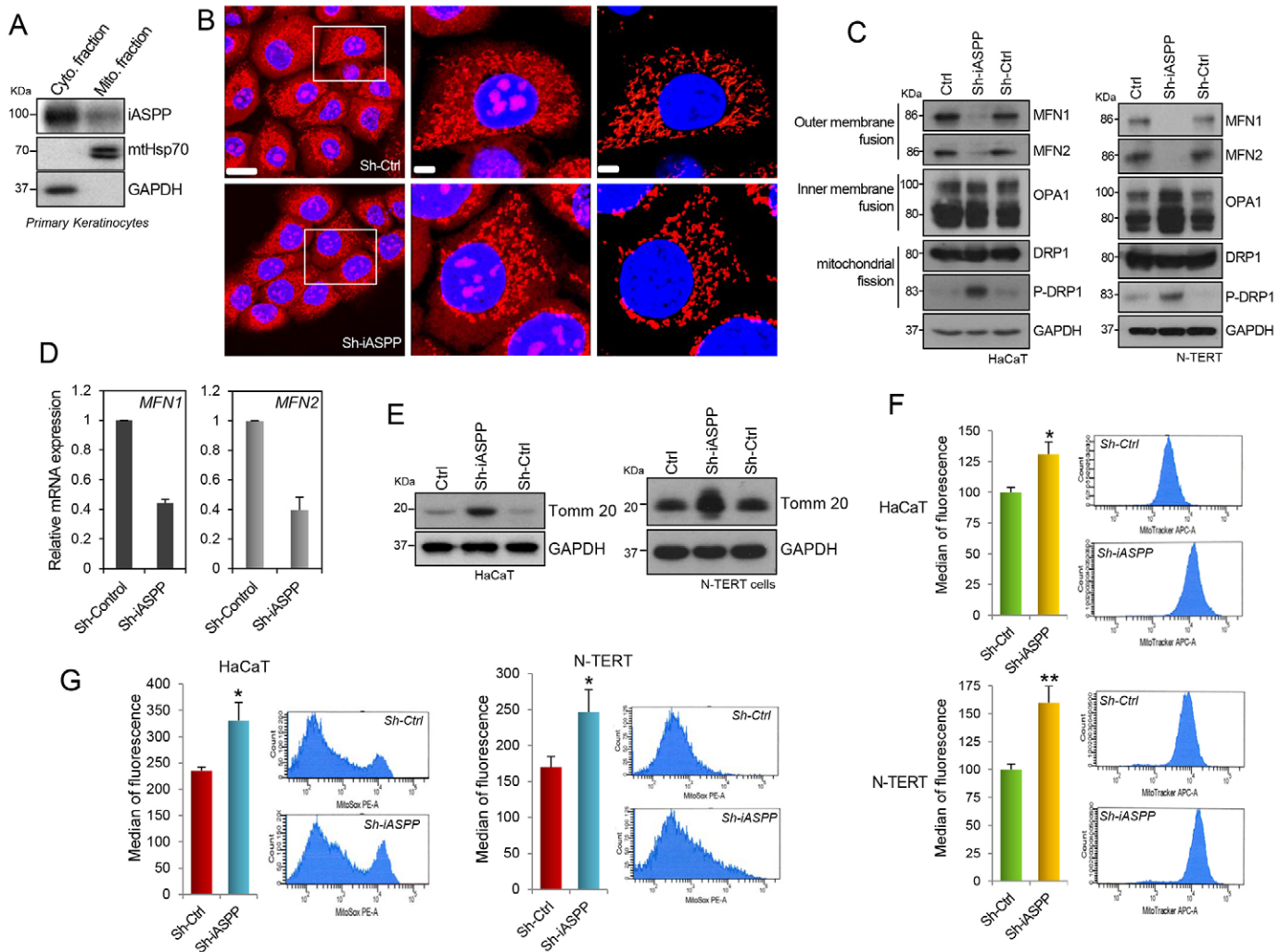


**Fig. 2. iASPP expression is crucial for shape, size and functional integrity of mitochondria.** (A) Western blot analysis of a cellular fractionation experiment, showing expression of iASPP in the mitochondria (mito.) and cytosolic (cyto.) fractions of primary keratinocytes. mtHsp70 and GAPDH were used as markers of mitochondrial and cytosolic compartments, respectively. (B) Confocal analysis of z-stack projections of HaCaT cells depleted of iASPP versus sh-Control (Ctrl), where the mitochondria were visualized with MitoTracker orange. DAPI (blue) is used as a nuclear stain. The white rectangle encloses an area shown at higher magnification in the middle panel, to show mitochondria. The right panels show a 3D-rendered image of mitochondria obtained with IMARIS software by applying a maximum-intensity mask to the MitoTracker channel. Scale bars: 20  $\mu$ m (left panel); 5  $\mu$ m (middle and right panels). (C) Western blot analysis of the effects of iASPP knockdown on the expression of fusion and fission proteins in HaCaT and N-TERT cells. GAPDH is shown as a loading control. (D) qRT-PCR analysis showing the effect of iASPP depletion from HaCaT cells on mRNA expression of MFN1 and MFN2. (E) Western blot analysis of mitochondrial outer membrane protein Tom20, which is upregulated in HaCaT and N-TERT cells depleted of iASPP. GAPDH is shown as a loading control. (F) Right, histograms representing live cells stained with DiIC<sub>1</sub>(5) in sh-control-treated and sh-iASPP-treated samples of HaCaT and N-TERT cells, by flow cytometry. Left, the median fluorescence intensity of MitoTracker orange staining in live cells, quantified from the right panels. Data show the median fluorescence intensity as mean  $\pm$  s.e.m for three independent experiments performed in triplicate. \* $P$ <0.05; \*\* $P$ <0.01 (two-tailed Student's  $t$ -test). (G) Histograms representing live cells stained for ROS using MitoSOX in HaCaT and N-TERT sh-control-treated and sh-iASPP-treated cells by flow cytometry. Bar charts to the left of each histogram show the median fluorescence intensity as mean  $\pm$  s.e.m for three independent experiments performed in triplicate. \* $P$ <0.05 (two-tailed Student's  $t$ -test).

Further morphological analysis showed that keratinocytes depleted for iASPP not only exhibited altered mitochondrial features but also displayed a more intense expression of the proteasomal and lysosomal proteins when compared with that of control cells. Decreased  $\alpha$ -tubulin expression and changes in microtubule orientation (more evident in N-TERT cells, supplementary material Fig. S2D) were also detected by immunostaining. Moreover, Golgi and endoplasmic reticulum (ER) proteins were less intensely expressed in keratinocyte cells depleted for iASPP, indicating an overall reduction in ER–cis-Golgi vesicular trafficking, as shown by reduced expression of the luminal ER retention marker, KDEL, and cis-Golgi matrix

protein GM130, respectively (Fig. 3B; supplementary material Fig. S2D).

All these cellular features are linked to intense metabolic signaling triggered by the depletion of iASPP. Increased expression of lysosomal and proteasomal components is normally documented during some stages of the autophagy process (Zhao et al., 2007), whereas decreased expression of Golgi and ER proteins could be the result of an excessive unfolded protein response (UPR). Mammalian target of rapamycin (mTOR), a crucial regulator of cell metabolism, growth and proliferation, physiologically controls translation in response to nutrients, energy levels and growth factors. Activation of mTOR complex 1 (mTORC1) stimulates

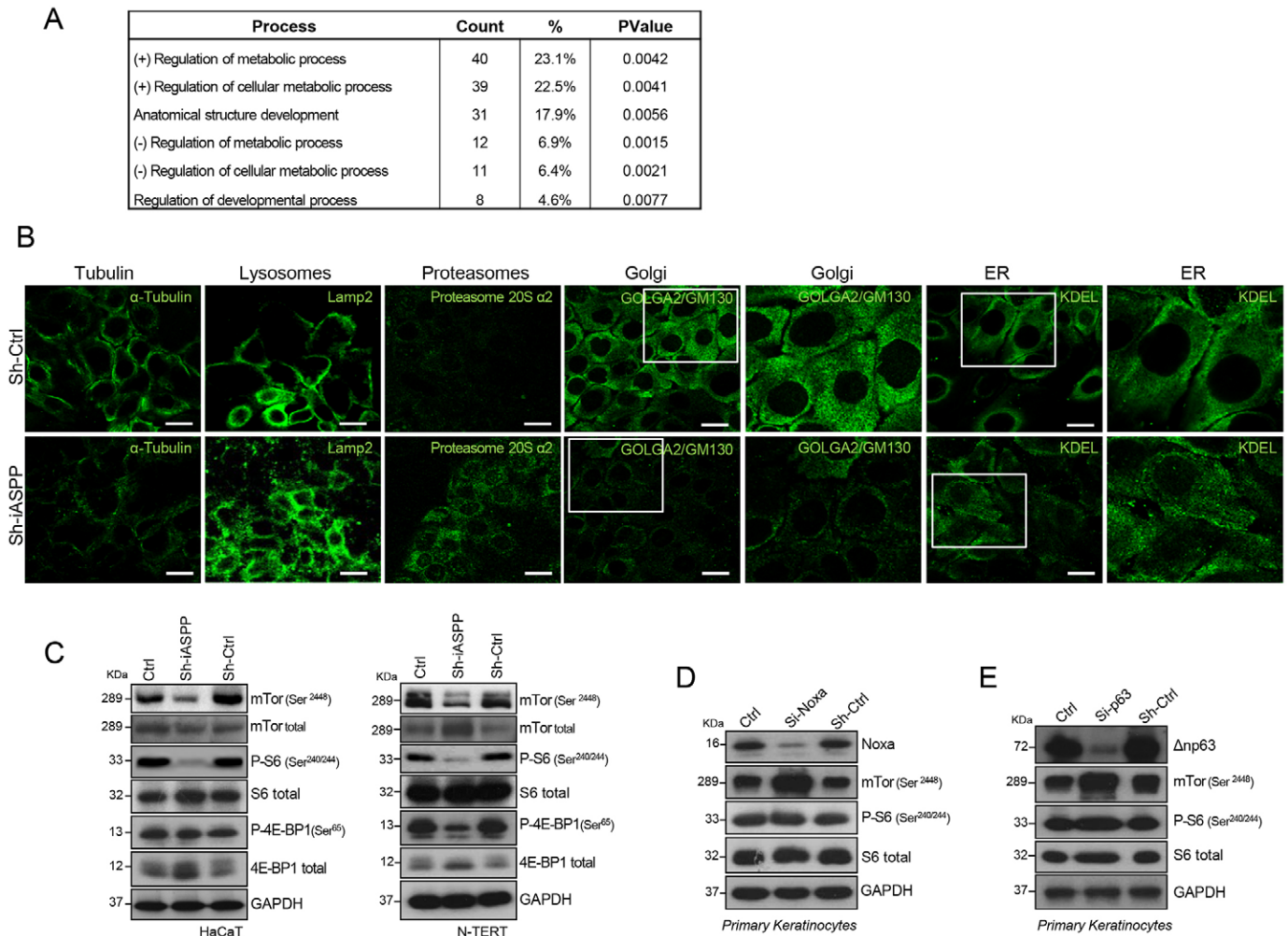


**Fig. 3. iASPP depletion changes the cytosolic architecture and induces metabolic stress.** (A) Functional annotation of genes affected by iASPP silencing. This analysis investigates the ontology of biological processes by using DAVID, a web-accessible program for the analysis of OMICS data. Biological processes with a  $P$ -value  $< 0.01$  are displayed. (B) Differential staining by immunofluorescence between the sh-control (Ctrl) and sh-iASPP cells. A proteasome marker (Proteasome 20S  $\alpha 2$ ) and a lysosome marker (Lamp2) are more highly expressed in sh-iASPP cells than in sh-Ctrl cells, whereas markers of microtubules ( $\alpha$ -tubulin), Golgi (cis-Golgi matrix protein, GM130) and ER (luminal ER retention marker KDEL) display a reduced expression in sh-iASPP cells, with microtubules also showing changes in orientation. White rectangles indicate areas that are shown as enlargements to the right. Scale bars: 20  $\mu$ m. (C) Western blot analysis showing that iASPP depletion impairs mTORC1 and reduces the expression of its downstream targets in HaCaT and N-TERT cells. (D) Western blot analysis of primary keratinocytes depleted of Noxa demonstrated that mTORC1 is unaffected by Noxa depletion. (E) Western blot analysis of primary keratinocytes depleted of p63 demonstrated that mTORC1 is unaffected by p63 depletion. For C–E, GAPDH was used as a loading control.

protein synthesis through its phosphorylation of p70-S6 kinase (p70-S6K, encoded by *RPS6KB1*) and 4E-BP1 (also known as EIF4EBP1). By contrast, starvation inactivates mTORC1, thereby inhibiting anabolic processes and liberating nutrient reserves with the induction of autophagy (Klionsky, 2009). Two different keratinocyte cell lines depleted of iASPP demonstrated deregulation of the mTORC1 signaling pathway, as shown by decreased expression of phospho-mTOR (Ser2448) and its downstream targets, such as phospho-RPS6 (Ser240/244) – whereas total levels of RPS6 were unaffected – or phospho-4E-BP1 (Ser65) (Fig. 3C). None of the previously described proteins that interact with iASPP in the regulation of homeostasis, such as p63 or Noxa, seemed to affect the mTORC1 signaling pathway, as depletion of Noxa (Fig. 3D) or p63 (Fig. 3E) in keratinocyte cultures did not affect the expression or phosphorylation of components of this pathway.

### Silencing of iASPP promotes autophagy in keratinocytes

Following on from the data shown in Fig. 1, which revealed that keratinocytes lacking iASPP unexpectedly displayed greater apoptotic resistance, we investigated whether this could be due to an induction of autophagy. Increased expression of exogenous beclin-1-GFP or LC3-GFP, as well as endogenous LC3, was detected in the iASPP-knockdown keratinocytes (supplementary material Fig. S3A–C). The process by which autophagosomes are converted into autophagolysosomes can be monitored by a method involving the use of LC3 tandemly tagged with GFP and monomeric (m)RFP (Kabeya et al., 2000; Kimura et al., 2007). In this method, transport of the tandem fluorescent-tagged LC3 (tFLC3) to the acidic environment of the lysosomes quenches the GFP but not mRFP signal, providing a tool for monitoring autophagosome traffic and lysosomal fusion. In control cells, GFP and mRFP signals colocalized, whereas, in cells depleted for iASPP, GFP levels decreased but a clear accumulation of the

tflLC3 punctate staining was observed with strong expression of the mRFP signal (Fig. 4A; supplementary material Fig. S3D). Control cells treated with rapamycin or that were serum-starved demonstrated a very similar pattern of tflLC3 fluorescence to the one displayed by iASPP-silenced keratinocytes. We then further examined the expression of several autophagy markers in keratinocytes treated with rapamycin (Fig. 4B) or depleted of iASPP (Fig. 4C; supplementary material Fig. S3E). Western blotting data showed that rapamycin treatment reduced the expression of endogenous iASPP and Noxa, precluding a cell death response in primary keratinocytes. The treatment reduced Mcl-1 expression, which is often reported in the early stages of autophagy, and upregulated beclin-1 and ULK1, both of which

are involved in a complex signaling pathway during autophagy induction. As a result of this activation, the expression of the lipidated form of LC3, LC3II, was also detected. Likewise, iASPP-silenced keratinocytes displayed increased protein expression of beclin-1, ULK1 and LC3II, coupled with downregulation of p62, indicating that the removal of iASPP from keratinocytes can induce productive autophagy (Claerhout et al., 2012), a cytoprotective metabolic process. Most of these key regulators, including lipidated LC3, showed the same expression pattern in another keratinocyte cell line (supplementary material Fig. S3E). By using western blotting, we further examined the expression of beclin-1 and LC3 in keratinocytes depleted of Noxa or p63. The results confirmed that

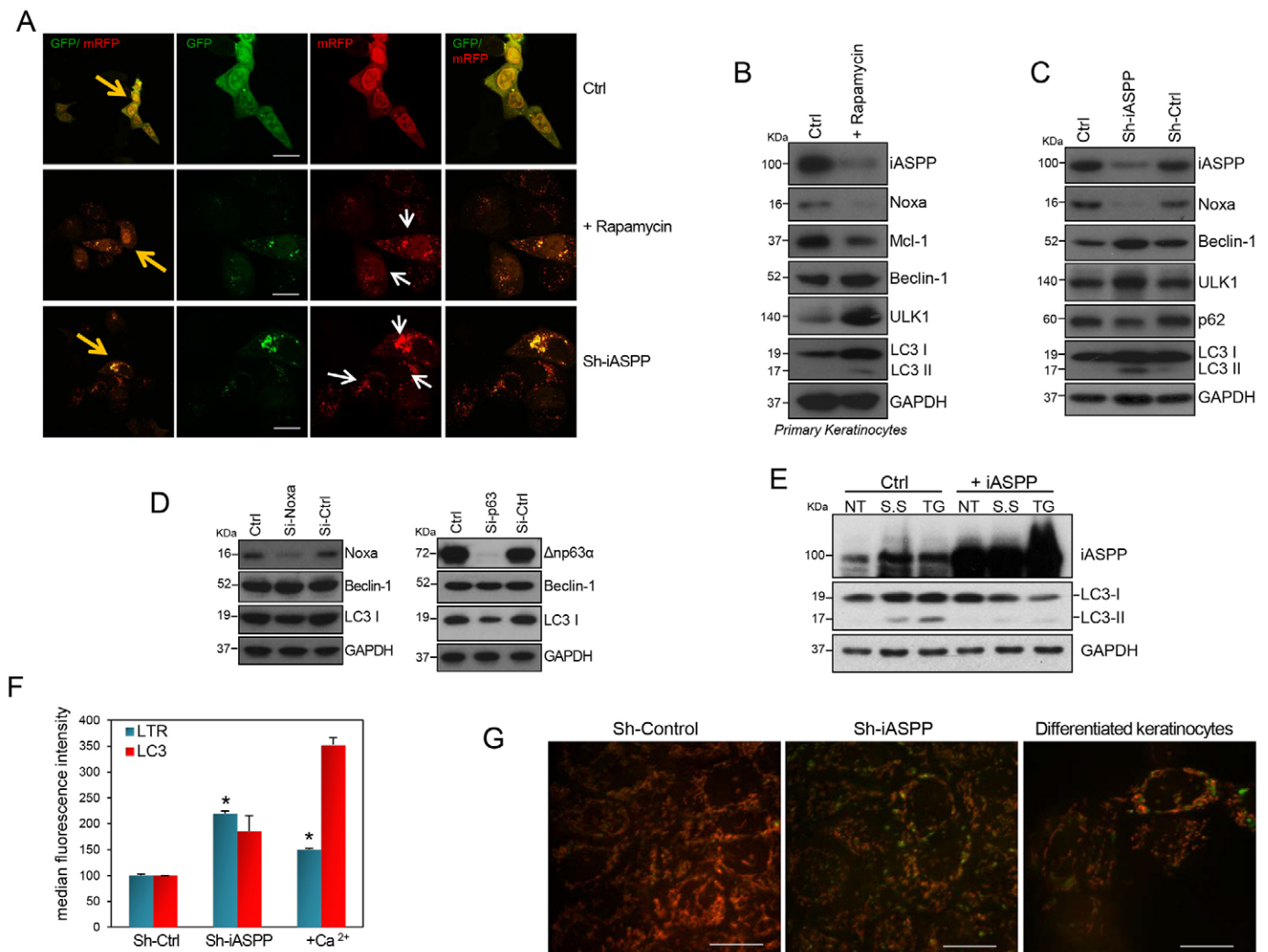


**Fig. 4. Silencing of iASPP promotes autophagy in keratinocytes.** (A) Confocal microscopy analysis of tflLC3 fluorescence in sh-control cells and sh-iASPP cells. Control (ctrl, without rapamycin) cells showed diffuse colocalization of GFP and mRFP. Rapamycin treatment for 24 h results in a strong expression of the plasmid in the sh-control cells, as determined by mRFP expression and the formation of puncta similar to those observed in the sh-iASPP cells. The orange arrows indicate the higher magnification of the analysed cells. The white arrows show the LC3 punctate staining. Scale bars: 20  $\mu$ m. (B) Western blot analysis showing the effects of rapamycin treatment on the expression of autophagic proteins in epidermal keratinocytes. (C) Western blots analysis of the effect of iASPP depletion on the expression of autophagic markers in HaCaT cells. (D) Western blot analysis revealing that the expression of autophagy markers was unaffected by the depletion of Noxa or p63 in primary keratinocytes. (E) Western blot analysis performed on HEK293 cells showing that iASPP overexpression inhibits the lipidation of LC3 after serum starvation (S.S, 4 h) or treatment with thapsigargin (TG, 2 h). NT, not treated (control cells). For B–E, GAPDH was used as a loading control. (F) Measurement of the fluorescence intensity of LysoTracker Green and LC3B in live cells, as determined by flow cytometric analysis of sh-control, sh-iASPP and differentiated (+Ca<sup>2+</sup>) HaCaT cells. Data show the median fluorescence intensity as mean  $\pm$  s.e.m for three independent experiments performed in triplicate. \* $P$ <0.05 (two-tailed Student's  $t$ -test). (G) Live imaging performed on sh-control, sh-iASPP and differentiated HaCaT cells. Cells were stained with LysoTracker Green and MitoTracker Orange. Scale bars: 20  $\mu$ m.

there was no activation of this autophagy pathway in response to the depletion of Noxa or p63, excluding their involvement in the regulation of this axis (Fig. 4D). Upregulation of iASPP in cells undergoing serum starvation or exposed to thapsigargin (an ER stress inducer that blocks  $\text{Ca}^{2+}$  reuptake by the ER and also acts as an inducer of AMPK-independent autophagy) abolished LC3 lipidation, thereby preventing the maturation and termination of the autophagy process and confirming the anti-autophagic role of iASPP (Fig. 4E; supplementary material Fig. S3F). We measured autophagic flux by flow cytometry using a specific anti-LC3B antibody and LysoTracker Red (LTR) staining to label the iASPP-depleted cells (Fig. 4F). This is a novel method, recently used to demonstrate that LTR specifically measures the lysosomal mass during autophagy and to show that an increase in the lysosomal mass is often associated with the upregulation of LC3B (Chikte et al., 2014). Overall, iASPP-silenced or differentiated keratinocytes demonstrated an increase in the LTR and LC3B signal. We further confirmed the flow cytometry data with live-cell imaging analysis using confocal microscopy (Fig. 4G). The resulting videos clearly showed a significant increase in LTG (LysoTracker Green) signal in both iASPP-depleted and  $\text{Ca}^{2+}$ -induced differentiated keratinocytes. Finally, we investigated autophagic flux by using bafilomycin A1 treatment. Our data confirmed that lysosome inhibition caused an almost 50% reduction in the autophagic flux in keratinocytes undergoing autophagy induced by either rapamycin or stable iASPP depletion. As a result of this block, LC3 turnover was impaired, with consequent increased LC3 expression due to lack of degradation (supplementary material Fig. S4A–C).

#### **iASPP forms a complex with Atg5–Atg12 and Atg16L1 proteins**

As the Atg5–Atg12 complex is required for the formation of autophagosomes and autolysosomes, we decided to investigate its expression and localization in human skin. The immunohistochemical analysis performed on adult human interfollicular epidermis revealed that Atg5–Atg12 partially colocalizes with cytoplasmic iASPP in the basal layer of the epidermis (Fig. 5A). To further explore a link between iASPP and autophagy, the interaction of iASPP with Atg5–Atg12 was examined. We tested for a possible interaction between iASPP and Atg5–Atg12 by immunoprecipitating keratinocyte cell lysates using a specific antibody against Atg5. The results showed that endogenous Atg16L1 (used as a positive control) and iASPP both co-immunoprecipitated with the Atg5–Atg12 complex (Fig. 5B). This interaction might be crucial, as the complex Atg5–Atg12–Atg16L1 is essential for the maturation stage of the canonical autophagy process and, in particular, for autophagosome formation. We overexpressed iASPP in HEK293 cells to establish whether increased iASPP levels could affect the expression of Atg5–Atg12 and Atg16L1 proteins. Increased iASPP expression did not alter the expression of Atg7 or Atg16L1, whereas it induced a downregulation of the Atg5–Atg12 protein complex (Fig. 5C). Likewise, depletion of iASPP in keratinocytes slightly increased the expression of Atg5–Atg12 without significantly affecting that of Atg7 or Atg16L1 (Fig. 5D). Furthermore, overexpression of iASPP in HEK293 cells affected the stability of the complex between Atg5, Atg12 and Atg16L1 by significantly decreasing the interaction of Atg16L1 with the Atg5–Atg12 complex (Fig. 5E). By contrast, the binding of endogenous Atg5–Atg12 to Atg16L1 significantly increased in both rapamycin-treated and iASPP-depleted keratinocytes (Fig. 5F). To further assess a possible

regulation of iASPP by Atg5–Atg12, primary keratinocytes were depleted of Atg5 using an siRNA construct, and western blots showed that the downregulation of Atg5 did not alter iASPP expression, thus excluding a possible feedback loop mechanism and also confirming the anti-autophagic role of iASPP even in the absence of Atg5 (Fig. 5G). Further analysis revealed that the expression of Atg7 protein was unaffected by Atg5 silencing, as Atg7 is upstream of Atg5, and also revealed that Rab9, a non-canonical autophagy effector involved in autophagosome formation, was highly expressed in keratinocytes even in the absence of Atg5. These data provide a novel mechanism by which iASPP can physiologically repress the interaction of Atg5–Atg12 with Atg16L1 in keratinocytes, thus inhibiting a crucial step of maturation during the autophagy process. Our data also reveal that a major block or impairment of the canonical autophagy pathway does not influence the expression of Rab9 (supplementary material Fig. S4E), suggesting the possibility of further alternative signaling pathways involved in autophagosome formation even in the keratinocyte lineage.

#### **Autophagy is crucial for keratinocyte differentiation**

In order to further explore how iASPP might affect the autophagy process within the epidermis, we measured LC3 expression in three dimensional (3D) organotypic culture, using control or iASPP-depleted keratinocytes. We have reported previously that this experimental skin model displays a premature differentiation program associated with concomitant loss of the proliferative compartment. In stratified epithelium derived from iASPP-silenced keratinocytes, LC3 expression was significantly increased compared with that observed in epithelium derived from sh-control-treated keratinocytes, and LC3 localized throughout the epithelium (Fig. 6A). Moreover, upon  $\text{Ca}^{2+}$ -induced differentiation, primary keratinocytes showed increased expression of keratin-1 (KRT1) and concomitant downregulation of  $\Delta\text{Np}63$  (Fig. 6B). In this monolayer model of differentiation, we not only confirmed the decrease in iASPP expression during differentiation, but we also observed the downregulation of important pro-apoptotic effectors, such as Noxa and Bak. More importantly, the cleavage and lipidation of LC3 was increased during keratinocyte differentiation. To further assess the reciprocal link between differentiation and survival processes, iASPP-depleted and  $\text{Ca}^{2+}$ -induced differentiated keratinocytes were exposed to UV-B at 10 mJ/cm<sup>2</sup>. An assessment of apoptosis performed using flow cytometry showed that iASPP-depleted cells and differentiated cells displayed similar degrees of apoptotic resistance upon treatment (Fig. 6C). By treating primary keratinocytes with increasing amounts of UV-B, we found that upregulation of the differentiation marker KRT1 correlated with the lipidation of LC3 (Fig. 6D), confirming that autophagy and differentiation processes are linked, at least in monolayer keratinocytes. Finally, treatment of  $\text{Ca}^{2+}$ -induced differentiated keratinocytes with the autophagy inhibitor 3-methyladenine (3-MA) provided evidence that inhibition of the autophagy process prevents the correct differentiation of keratinocytes (Fig. 6E). The reduction in the levels of phospho-RPS6 in the proliferating cells confirmed the effectiveness of 3-MA. However, treatment of the differentiated cells with 3-MA did not affect phospho-RPS6 expression, whereas it led to accumulation of KRT14 and reduced KRT1 levels, with consequent loss of LC3 lipidation. Finally, keratinocytes depleted for Atg5 by RNA interference were induced to differentiate (Fig. 6F). This further approach of blocking Atg5-dependent autophagy once more confirms the impairment of differentiation in monolayer keratinocytes in which autophagy

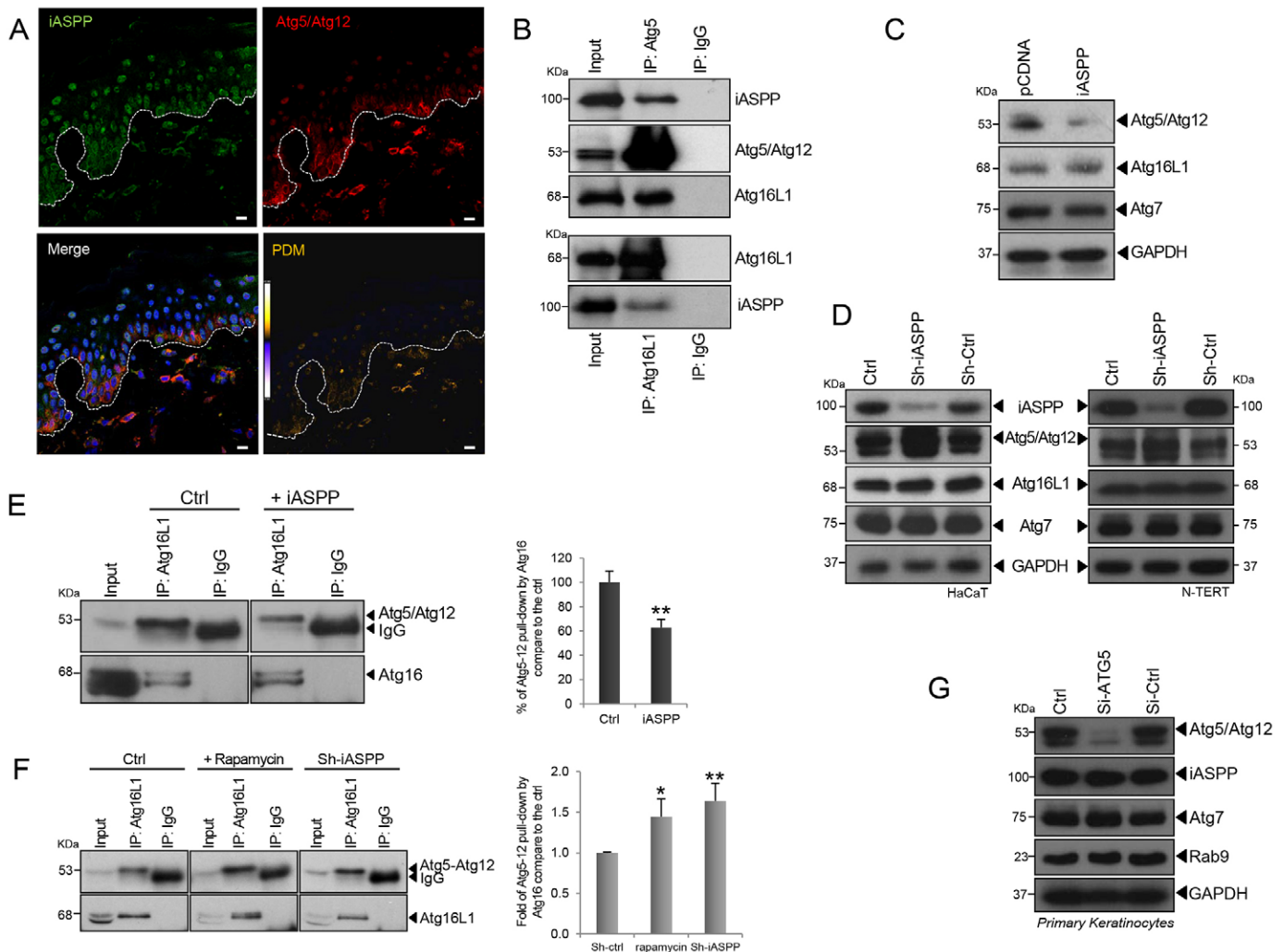


**Fig. 5. iASPP forms a complex with Atg5–Atg12 and Atg16L1 proteins.** (A) Localization of Atg5–Atg12 and iASPP in human adult skin by confocal microscopy. Pseudocolored ‘product of the differences from the mean’ (PDM) images, in which each pixel is equal to the PDM value at that location, are shown with a PDM scale. White dotted lines represent the dermal-epidermal junction. Scale bars: 20  $\mu$ m. (B) Co-immunoprecipitation demonstrating the binding between iASPP, Atg5–Atg12 and Atg16L1 in HaCaT cells, the total lysates of which were immunoprecipitated (IP) with an anti-Atg5–Atg12 or an anti-Atg16L1 antibody. Atg5–Atg12, Atg16L1 and iASPP levels were analyzed by western blot analysis. (C) Western blot analysis of HEK293 cells shows that overexpressing iASPP results in reduced Atg5 but not Atg16L1 protein expression. (D) Knockdown of iASPP in HaCaT and N-TERT cells results in an increase in Atg5 expression but no variation in Atg16L1 or Atg7 protein expression compared with that of mock-transfected (Ctrl) cells or sh-Ctrl cells. (E) Co-immunoprecipitation experiments performed in HEK293 cells indicate that overexpression of iASPP reduces the interaction between Atg5–Atg12 and Atg16L1. The total lysates were immunoprecipitated with an anti-Atg16L1 antibody. Atg5–Atg12 and Atg16L1 levels were analyzed by western blot analysis. The percentage of Atg5–Atg12 in complex with Atg16L1 was calculated as described in the Materials and Methods. (F) Co-immunoprecipitation demonstrating that both depletion of iASPP and rapamycin treatment enhance the interaction between endogenous Atg5–Atg12 and Atg16L1 in HaCaT cells. The total lysates were immunoprecipitated with an anti-Atg16L1 antibody. Atg5–Atg12 and Atg16L1 levels were analyzed by western blot analysis. The percentage of Atg5–Atg12 in complex with Atg16L1 was calculated as described in the Materials and Methods. For E and F, results represent the mean  $\pm$  s.e.m. (three independent experiments); \* $P < 0.05$ ; \*\* $P < 0.01$  (two-tailed Student’s *t*-test). (G) Western blot analysis reveals that Atg5 depletion in HaCaT cells does not affect iASPP, Atg7 or Rab9 protein expression.

is blocked. Atg5-depleted cells were unable to increase KRT1 expression and LC3 lipidation during  $\text{Ca}^{2+}$ -induced differentiation. Our data therefore consolidate the interdependency of autophagy and differentiation in human epidermal keratinocytes.

To establish whether autophagosome formation was a crucial step for skin stratification, we pharmacologically blocked autophagy in the organotypic 3D culture model. Our data showed that 3-MA treatment reduced stratification of the epidermis in skin reconstituted with both sh-iASPP and sh-control keratinocytes (Fig. 7A,B). Confocal immunofluorescence confirmed the decreased expression of markers of terminal differentiation, such

as loricrin and involucrin in the 3-MA-treated skin reconstructs. However, the skin was positive for KRT1, the expression of which corresponds to the spinous layer. These observations suggest that treatment with 3-MA specifically affects those cells in transition between spinous and granular layers within sh-iASPP skin reconstructs and therefore reducing the stratification process. Moreover, for the sh-control keratinocytes, treatment with 3-MA maintained the proliferative compartment of the skin (Fig. 7C,D). Interestingly, the level of Rab9 expression slightly increased in the iASPP-depleted skin reconstructs even upon 3-MA treatment (supplementary material Fig. S4D,E), confirming the presence of

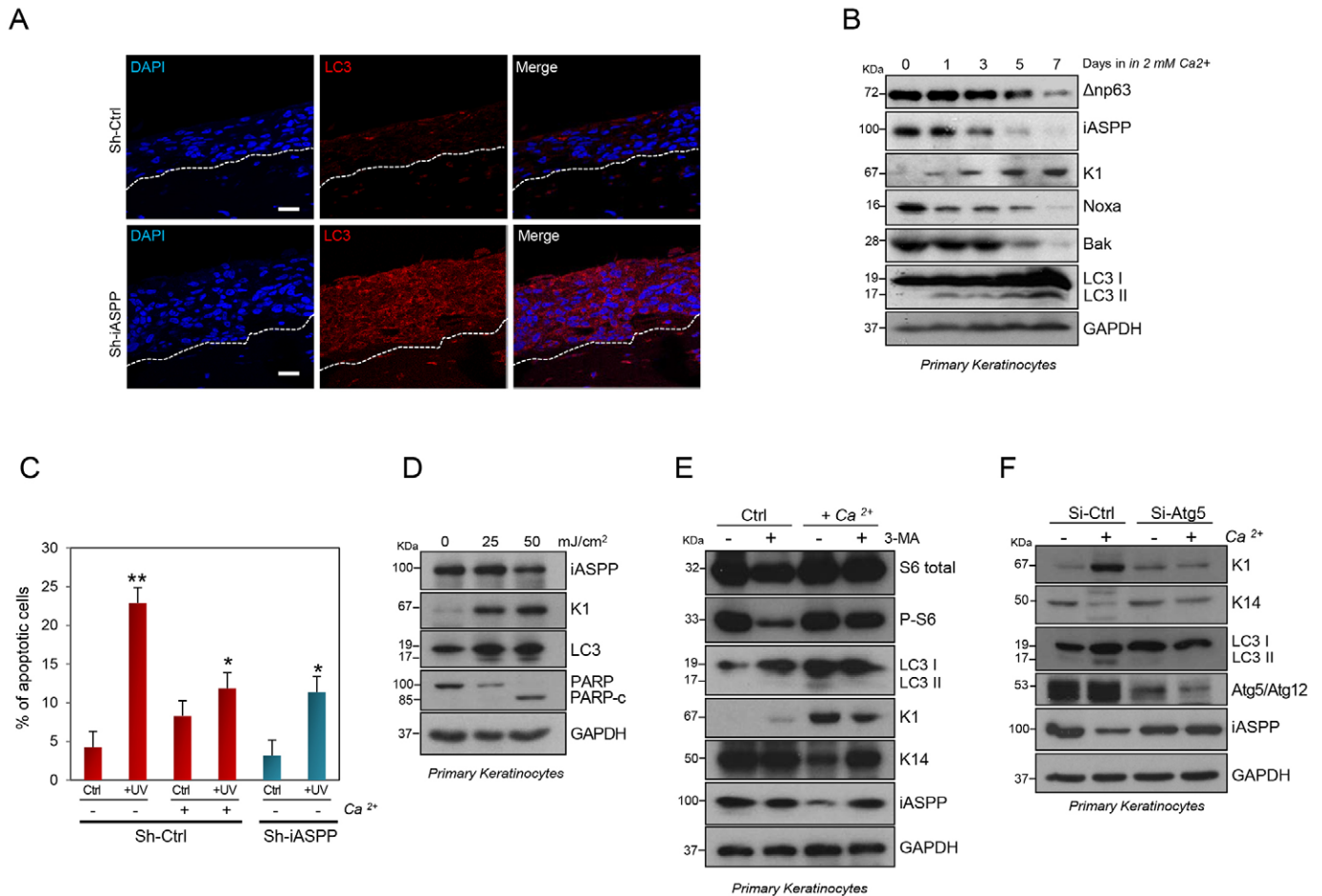


**Fig. 6. Autophagy is essential for differentiation in keratinocytes.** (A) Immunofluorescence staining confirms that iASPP silencing induces LC3 expression in iASPP-knockdown skin-graft sections. DAPI (blue) is used as a nuclear marker. The white dotted line represents the dermal-epidermal junction. Scale bars: 20  $\mu$ m. (B) Western blot analysis showing the expression of markers of apoptosis and differentiation during Ca<sup>2+</sup>-induced differentiation in monolayer primary keratinocytes. KRT1 (K1) was used as marker to confirm differentiation. (C) Apoptosis assay performed on iASPP-silenced HaCaT cells versus control or differentiated keratinocytes, treated with 10 mJ/cm<sup>2</sup> UV-B. Cell death (% apoptotic cells) was quantified using flow cytometric analysis of annexin-V- and DAPI-positive populations. Results represent the mean  $\pm$  s.e.m. (three independent experiments); \* $P$ <0.05; \*\* $P$ <0.01 (two-tailed Student's  $t$ -test). (D) Western blot analysis of iASPP, KRT1, LC3 and PARP expression in UV-B-irradiated primary keratinocytes treated with 0, 25 and 50 mJ/cm<sup>2</sup> of UV-B. PARP cleavage indicates the UV-B dose inducing apoptosis. (E) Western blot analysis showing the expression of markers of autophagy and differentiation in human primary keratinocytes treated with 3-MA (5 mM for 24 h) upon treatment with Ca<sup>2+</sup> (1.2 mM for 48 h). (F) Western blot analysis of the expression of markers of autophagy and differentiation in si-Ctrl-treated and si-Atg5-treated keratinocytes upon treatment with Ca<sup>2+</sup> (1.2 mM for 48 h). For B and D–F, GAPDH was used as a loading control.

alternative Atg5- and Atg7-independent pathways involved in autophagosome formation in this 3D model. Our findings underscore the importance of autophagosomes in the process of skin development. Ultimately, our model reveals that, at least in human skin, blocking one crucial step of the autophagy program is sufficient to compromise the differentiation pathways and, consequently, epithelial stratification.

## DISCUSSION

Our study (the results of which are summarized in Fig. 7E) explores the contribution of iASPP to the apoptotic cell death response. We have recently shown that iASPP is involved in the maintenance of epidermal homeostasis, regulating genes that are essential for the cell adhesion, differentiation and proliferation of stratified epithelia (Chikh et al., 2011). Here, we have reinforced the notion of a constitutive anti-apoptotic function of iASPP, the expression of which is sufficient to repress apoptosis. We have also shown here for the first time that the depletion or possible

downregulation of iASPP (which might occur at some stage in skin diseases) can trigger a productive form of autophagy, a metabolic pathway also aimed at protecting against cell death.

Our data reveal that keratinocytes depleted of iASPP failed to display greater apoptotic sensitivity when exposed to DNA damaging agents. It is well established that, in cancer, iASPP has an oncogenic function, and in several cancer cell lines its experimental silencing promotes apoptosis (Cai et al., 2012; Jiang et al., 2011; Li et al., 2012; Liu et al., 2009; Liu et al., 2008; Pang et al., 2010; Zhang et al., 2011). However, our data are consistent with a previous report that, in non-transformed cells (primary cultures of lymphocytes and fibroblasts), treatment with iASPP-specific siRNA reduced levels of apoptosis (Laska et al., 2007). Moreover, iASPP depletion reduces cell proliferation (Chen et al., 2010; Chikh et al., 2011; Li et al., 2011; Lu et al., 2010; Notari et al., 2011; Zhang et al., 2011), and it is known that slowly proliferating cells are more resistant to cytotoxic agents than rapidly proliferating cells (Sultana et al., 2003).

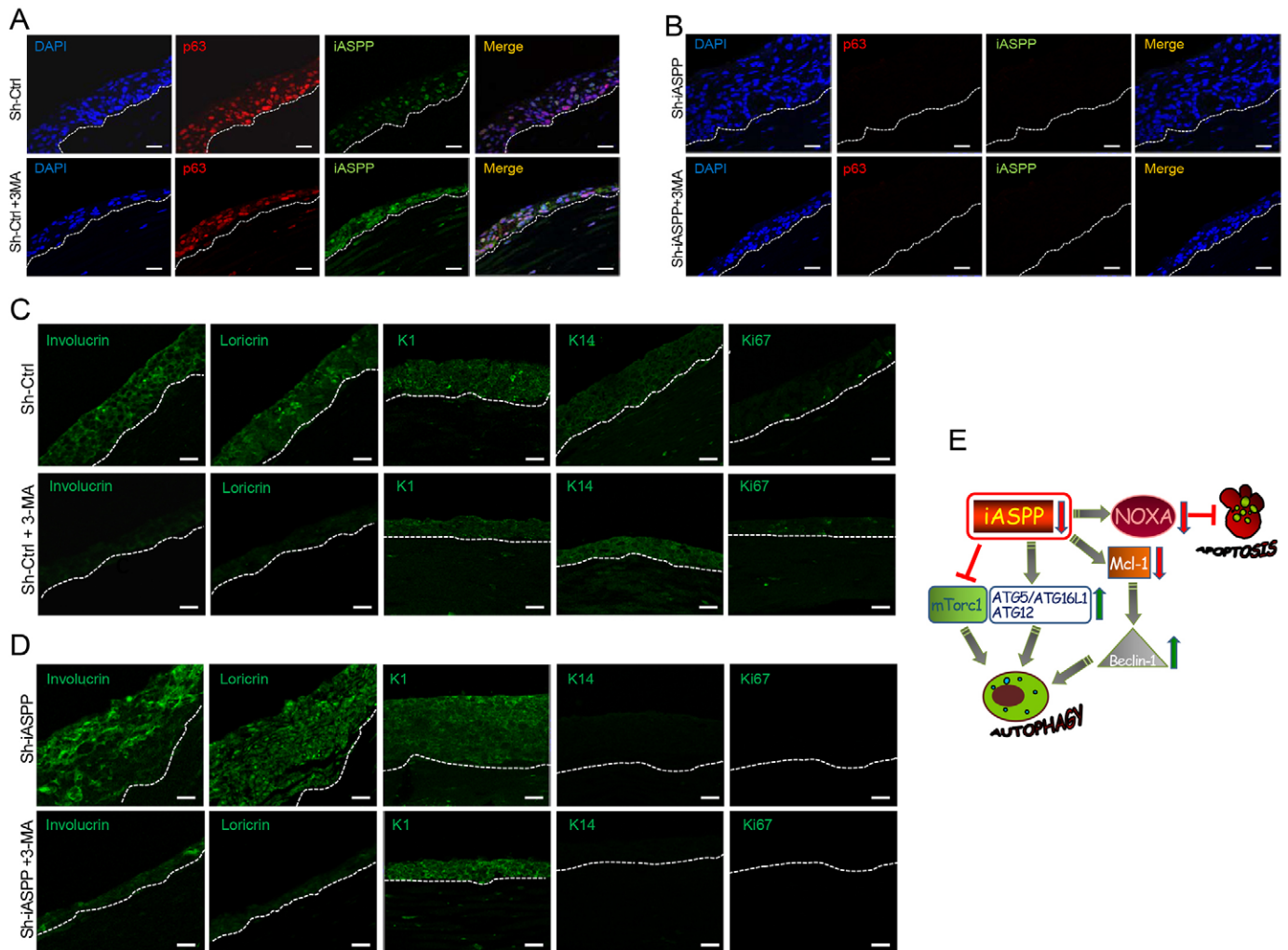


**Fig. 7. Depletion of iASPP induces differentiation through autophagy.** (A) Confocal analysis showing the expression of p63 (a marker of the basal layer of the epidermis) and iASPP in sections of sh-control 3D organotypic cultures. By contrast, keratinocytes treated with 3-MA display impairment in the stratification of the epidermis, but maintain the expression of p63 and iASPP in the basal layer of the epidermis. The dotted line represents the dermal-epidermal junction. Scale bar: 20  $\mu$ m. (B) Immunofluorescent staining confirms that silencing of iASPP results in the loss of p63 expression from the skin graft sections. 3D organotypic cultures treated with 3-MA display impaired stratification of the epidermis in the absence of p63 expression. In A and B, DAPI (blue) is used as a nuclear marker. The dotted line represents the dermal-epidermal junction. Scale bar: 20  $\mu$ m. (C) In sh-scramble sections, markers of differentiation, including KRT1 (K1), loricrin and involucrin are detectable, and the samples display the normal basal layer expression of KRT14 (K14) and expression of proliferative markers, such as Ki67. By contrast, in sh-scramble sections treated with 3-MA, the markers of terminal differentiation are downregulated, but these samples display the normal expression of KRT1 and proliferative markers, such as KRT14 and Ki67. The dotted white lines represent the dermal-epidermal junction. (D) Sections containing keratinocytes silenced for iASPP. In these samples, the markers of differentiation are induced in all of the epidermis, whereas basal layer and proliferation markers were downregulated, highlighting the disorganization of the basal layer and the presence of terminally differentiating cells. By contrast, sh-iASPP sections treated with 3-MA display downregulation of terminal differentiation markers, with maintenance of the expression of KRT1. Scale bars: 20  $\mu$ m. (E) Diagram illustrating how iASPP expression in keratinocytes can affect important physiological activities.

Several studies have highlighted the complexities of how Bcl-2 proteins dictate cellular fate (Chipuk and Green, 2008; Tait and Green, 2010). We found that iASPP is present in the mitochondria and its depletion can affect the balance between Bcl-2 protein interactions. In particular, iASPP depletion induces a drastic downregulation of *NOXA*, a pro-apoptotic gene of the Bcl-2 family, the expression of which is essential for UV-B-induced apoptosis in keratinocytes (Naik et al., 2007; Nys et al., 2010; Villunger et al., 2003). Our data suggest that reduced iASPP expression is able to switch off the apoptotic pathway through Noxa depletion, and turn on autophagy. The effect on Bak expression is more likely to be cell-type specific and requires further exploration. The induction of autophagy is coupled with the dissociation of beclin-1 from Bcl-2, Bcl-xL or Mcl-1 (Maiuri et al.,

2007). However, our data show an increase in the expression of beclin-1 and a decrease in Mcl-1 in cells depleted for iASPP. It has been reported that the binding between beclin-1 and Bcl-2 might reduce the extent of autophagy but not affect protection against apoptosis (Ciechomska et al., 2009). Our data suggest that decreased Mcl-1 expression might allow the release of beclin-1 to induce the initial steps of autophagy. Indeed, the depletion of Mcl-1 has already been linked with the activation of autophagy during neuronal development (Germain et al., 2011). Noxa can complex with Mcl-1, controlling the stability of the latter (Lowman et al., 2010). Therefore, we speculate that, in a homeostatic context, such as that of the epidermis, iASPP depletion reduces Noxa expression, which could contribute to turning off Mcl-1 and switching on the autophagy pathway.

In our previous report, we demonstrated that the junctional integrity complex is disrupted in iASPP-depleted keratinocytes (Chikh et al., 2011). Here, we further investigate the morphology of the cytosolic structure and we identify a remarkable phenotype. We firstly establish that iASPP expression is crucial to the processes regulating mitochondrial function, namely fission and fusion. The mitochondria are dynamic organelles that migrate throughout the cell, fuse, divide and undergo regulated turnover (Chen and Chan, 2009). iASPP depletion affects the balance of these activities by inhibiting the fusion machinery, leading to the formation of numerous small sphere-shaped mitochondria instead of the tubular and branched organelles observed in normal control cells (Gomes and Scorrano, 2013). A similar phenotype has been reported for the mitochondria of quiescent cells, which have been described as containing numerous morphologically and functionally distinct small spheres (Collins et al., 2002). We also confirm the same mitochondrial morphology in differentiated keratinocytes. We cannot exclude at this stage that iASPP might require other types of binding partner to perform all of its effects on the mitochondrial fission-fusion cycle, but at least we can exclude Noxa, Bak and Mcl1, whose expression could be influenced by iASPP silencing in keratinocytes. Specific depletion of each of these proteins did not affect iASPP expression, excluding any feedback loop with iASPP in these cells, but depletion of each of these proteins also was not sufficient to modulate the fine-tuning of the mitochondrial fission-fusion cycle. Moreover, iASPP depletion impairs mitochondrial degradation, with consequent accumulation of mitochondria and increase of mitochondrial mass. Further analysis of the mitochondrial membrane potential also showed that these cells feature hyperpolarized mitochondria. Mitochondrial hyperpolarization shifts energy production towards the cytoplasm, leading to apoptotic resistance (Bonnet et al., 2007), which is often reported as a characteristic of the autophagy process (Paglin et al., 2005). However, keratinocytes depleted for iASPP not only have altered mitochondria but also display increased expression of proteasomal and lysosomal compartments. By contrast, tubulin, Golgi proteins and ER proteins are less extensively expressed, and the compartments show an overall disorganization. We interpret these cellular features as a consequence of intense metabolic signaling triggered by the depletion of iASPP. Increased expression of lysosomal and proteasomal components has been documented during autophagy (Zhao et al., 2007). Decreased expression of Golgi and ER proteins could be the result of an excessive UPR, a cellular stress response related to the ER that is implicated in both pro-survival responses, by maintaining cellular homeostasis, and in apoptotic cell death, when these responses are not sufficient to relieve ER stress (Kim et al., 2006; Milani et al., 2009). Activation of the UPR has been reported during normal epidermal keratinocyte differentiation (Sugiura et al., 2009). Thus, deregulated UPR activity could be predicted in the absence of iASPP, although further experiments are needed to explore this hypothesis.

Mammalian target of rapamycin (mTOR), a crucial physiological regulator of cell metabolism, growth and proliferation, controls translation in response to nutrients, energy levels and growth factors. By contrast, starvation inactivates mTORC1, thereby inhibiting anabolic processes and liberating nutrient reserves with the induction of autophagy (Klionsky, 2009). We report that keratinocytes depleted of iASPP display compromised expression of mTORC1, as well as several of its downstream targets. Molecular analysis of autophagic markers in

these cells confirms not only increased beclin-1 and ULK1 expression, but also increased p62 degradation and, more importantly, lipidation of LC3-II. This was further validated by monitoring autophagic flux using tandem RFP- and GFP-tagged LC3 (Mizushima et al., 2010), a fusion protein in which the mRFP signal is visible during fusion with lysosomes, indicating a normal autophagic maturation process. Furthermore, mitochondrial dysfunction can also compromise mTORC1 signaling (Lee et al., 2012), with consequent increased production of ROS. Recent reports suggest a regulatory role of ROS as signaling molecules in autophagy, linking them to either cell survival or cell death (Bellot et al., 2013; Lee et al., 2012). However, the molecular mechanism implicating ROS in the induction of autophagy remains elusive (Bellot et al., 2013). Our data reveal increases in ROS production in both iASPP-silenced and differentiated keratinocytes. Previous studies have established that differentiation-related changes, including induction of a flattened morphology, stratification and keratin-10 expression, were a consequence of ROS production (Tamiji et al., 2005). Our findings identify that UV-B exposure promotes the appearance of differentiation markers in keratinocytes. Interestingly, our data also demonstrate that the differentiated cells share the same features of autophagy as cells depleted for iASPP.

The autophagy pathway requires autophagosome formation and maturation, and Atg5 is an essential component of the maturation process (Mizushima et al., 2003; Mizushima et al., 2001). Atg5 constitutively conjugates with a ubiquitin-like protein, Atg12, forming a complex with Atg16L1. The Atg5–Atg12–Atg16L1 complex localizes to nascent autophagosomes and is essential to initiate the autophagosome maturation process. Immunoprecipitation experiments reveal the ability of iASPP to complex and affect the dynamics of Atg5–Atg12 and Atg16L1. Increased iASPP expression reduces the formation of the Atg5–Atg12–Atg16L1 complex and prevents LC3 lipidation in human keratinocytes. Conversely, iASPP depletion significantly increases the amount of Atg5–Atg12 that is able to interact with Atg16L1, providing at least one possible link with the autophagy maturation process. This is supported by the fact that, in human epidermis, cytoplasmic iASPP partly colocalizes in the basal epidermal layer with endogenous Atg5–Atg12. A recent report has shown that ASPP2 can also compete with Atg16L1 for Atg5–Atg12 binding, preventing the formation of the Atg16L1–Atg5–Atg12 complex, thus inhibiting RAS-induced autophagy (Wang et al., 2012). In the same report, silencing of iASPP failed to show any induction of RAS-dependent autophagy. This could be due to the use of a specific cancer cellular model (this work used HKe3 ER:HRAS V12 cells, isogenic counterparts of HCT116 cells transduced with a mutant HRAS fused to the estrogen-receptor-ligand-binding domain). One of the aims of our study was to define the role of iASPP in the DNA damage response in a physiological context in humans, such as in epidermal keratinocytes. Further experiments will be needed to assess whether the anti-autophagy function of iASPP might be lost or modulated during cancer progression and in which specific cancer cell lineage this might occur.

Our data highlight the interdependency between autophagy and differentiation in keratinocytes. Pharmacological blocking of autophagy by 3-MA or by RNAi-mediated Atg5 depletion results in an impairment of differentiation in keratinocyte monolayer experiments, confirming recent results in adult skin stem cells (Salemi et al., 2012). We translated our findings in an organotypic skin model to challenge putative *in vivo* effects of autophagosome

formation during the development of the epidermis. 3-MA treatment prevents epidermal stratification even in skin reconstructs composed of iASPP-depleted keratinocytes. The premature differentiation process previously shown in the absence of iASPP was abrogated, indicating that autophagosome formation is required for normal stratification of the epidermis. Depletion of iASPP increases the expression of Atg5–Atg12 in human keratinocytes. Results obtained from a recent mouse model show that increased Atg5 expression activates autophagy and increases resistance to cell death (Pyo et al., 2013). Although *Atg5* and *Atg7* are believed to be essential genes for mammalian macroautophagy, recent studies highlight the discovery of an Atg5- and Atg7-independent alternative pathway in mice (Nishida et al., 2009; Shimizu et al., 2010) and an Atg3- and Atg7-independent pathway in flies (Chang et al., 2013). Autophagy can still occur in *Drosophila* cells through LC3 (Atg8), even in the absence of Atg3 or Atg7. In another cellular model (MEFs) lacking Atg5 or Atg7, autophagosome-autolysosome formation can still occur, even without LC3 lipidation, but instead in a Rab9-dependent manner, by the fusion of isolated membranes with vesicles derived from the trans-Golgi and late endosomes. These alternative pathways should partially explain a recent report showing that impairment of autophagy in a mouse model does not prevent the development of a functional epidermal barrier (Rossiter et al., 2013). Discrepancies with our data could further be explained by the use of mouse models, whereas our study has been performed with human epidermal keratinocytes. Interestingly, although 3-MA treatment of our skin reconstructs blocks the canonical Atg5/Atg7-dependent autophagy pathway, it does not prevent increased Rab9 expression, even in the absence of iASPP. Our report therefore confirms the existence of an alternative Atg5/Atg7-independent autophagy pathway in human epidermis.

In summary, our data reinforce the concept that autophagy is a normal physiological process required during differentiation of the skin, and that the interplay between apoptosis and autophagy has an essential role in epidermal homeostasis. Importantly, we show that iASPP participates in the homeostasis of human epithelia by influencing this balance between apoptosis and autophagy. Here, we have highlighted the constitutive anti-apoptotic nature of iASPP, the expression of which is sufficient to repress apoptosis. In addition, we show that its depletion or downregulation can trigger a productive form of autophagy, i.e. a cytoprotective metabolic pathway. Ultimately, this study provides an alternative mechanism to explain how epithelial integrity is maintained even following exposure to (environmental) stressors, such as UV radiation, and might also improve our understanding of the etiology of skin diseases that are characterized by defects in differentiation and DNA damage responses.

## MATERIALS AND METHODS

### Cell lines, culture conditions, transfection and reagents

Human epidermal keratinocytes were purchased from Gibco (Invitrogen, Paisley, UK). HaCaT cells were cultured in DMEM supplemented with 10% fetal bovine serum (FBS) and 1% penicillin-streptomycin. N-TERT cells were cultured in DMEM:F12 medium supplemented with 20% FBS, 1% glutamine, 50 µg/ml gentamicin, 100 µM tissue plasminogen activator (TPA), 2 µg/ml human stem cell factor (hSCF), 0.1 µM cholera toxin and 10 µM endothelin. HEK293 cells were transfected by using Lipofectamine 2000 reagent (Invitrogen) at a 1:2 (µl/µg) ratio with DNA, using 5 µg of plasmid DNA. Downregulation of iASPP in HaCaT and N-TERT cells was performed as described previously (Chikh et al., 2011). Cells were treated with UV-B as indicated in the figure legends. Thapsigargin and 3-MA were purchased from Sigma (Poole, UK). LY-294002 was purchased from Calbiochem.

### Organotypic cultures

Organotypic cultures on collagen:Matrigel gels were performed as described previously (Chikh et al., 2011), with some modifications. Collagen:Matrigel gels were prepared by mixing 3.5 volumes of type-I collagen (First Link, UK), 3.5 volumes of Matrigel (BD Biosciences, UK), 1 volume of 10× DMEM, 1 volume of FCS and 1 volume of DMEM with 10% FCS and human foreskin fibroblasts (resuspended at a density of  $5 \times 10^6$  cells/ml). A total of 1 ml of the gel mixture was placed into each well of a 24-well plate and allowed to polymerize at 37°C for 1 h. After polymerization, 1 ml of DMEM was added to each well, and the gels were incubated for 18 h to equilibrate. Keratinocytes (shRNA-iASPP treated, shRNA-scramble and control) were seeded into a plastic ring placed on the top of the gel at a density of  $5 \times 10^5$  cells per gel. After 24 h, the rings were removed and gels were raised to the air–liquid interface on stainless steel grids. The gels were harvested at day 14 and frozen at –80°C.

### Analysis of apoptosis

Apoptosis was assessed by flow cytometry by using annexin V and propidium iodide staining. Cells were washed in PBS, trypsinized, pelleted and resuspended in 400 µl of binding buffer (Becton Dickinson, San Jose, CA), samples were incubated with 2 µl of annexin-V-FITC (Becton Dickinson) for 15 min at room temperature, then propidium iodide (5 µg/ml) was added to the sample.

### Immunofluorescence

Cultured cells were plated onto glass coverslips at a density of 150,000 cells/cm<sup>2</sup> in 12-well culture plates for 24 h. Cells were washed in PBS, fixed in 4% formaldehyde in PBS for 10 min at room temperature, washed twice in fresh PBS, permeabilized with 1% Triton X-100 (Sigma) in PBS for 3 min at room temperature and blocked with 5% FBS in PBS for 30 min at room temperature. Cells were incubated with antibodies diluted in 5% FBS in PBS overnight at 4°C, followed by incubation with secondary antibodies conjugated with Alexa Fluor (Molecular Probes) diluted in 5% goat serum in PBS for 1 h. Nuclei were stained with 4,6-diamidino-2-phenylindole, dihydrochloride (DAPI, Molecular Probes). Coverslips were mounted onto microscope slides using Vectashield Mounting Medium (Vector Laboratories). Fluorescence was evaluated by confocal microscopy. Immunohistochemistry was performed on frozen tissue; sections were air-dried and stored at 4°C overnight before being processed. Tissues were fixed in acetone at –20°C for 10 min. Sections were washed three times with PBS. Then they were incubated with primary antibodies overnight at 4°C. Sections were washed three times with PBS and incubated with the secondary antibodies conjugated with Alexa Fluor (Molecular Probes) for 30 min at room temperature. After two washes, the sections were incubated for 10 min with DAPI to reveal the nuclei. Then, the tissue sections were mounted using Vectashield Mounting Medium (Vector Laboratories). Fluorescence was evaluated by confocal microscopy. A pseudocolored ‘product of the differences from the mean’ (PDM) image was calculated by the program as: PDM=(red intensity–mean red intensity)×(green intensity–mean green intensity).

### Fluorescence imaging of mitochondria

Cultured cells were plated onto glass coverslips at a density of 150,000 cells/cm<sup>2</sup> in 12-well culture plates and allowed to attach overnight at 37°C. The next day, the medium was discarded and replaced with medium containing MitoTracker Orange (CMTMRos, Molecular Probes, 40 nM). Cells were incubated with MitoTracker Orange for 30 min prior to washing twice in PBS. Cells were fixed in 1 ml of 4% formaldehyde in PBS for 10 min at room temperature, washed twice in fresh PBS (5 min per wash) and stored at 4°C in PBS. Nuclei were stained with DAPI (Molecular Probes). Coverslips were mounted onto microscope slides using Vectashield Mounting Medium (Vector Laboratories). Fluorescence was evaluated by confocal microscopy.

### Autophagic flux quantification

Measurements of autophagic flux in mCherry-GFP–LC3 were performed using an imaging-based assay as reported previously (Nyfeler et al.,

2012). We quantified the total number of autophagic vacuoles (including early autophagosomes and autolysosomes) per cell soma. These were quantified on the red channel, as mCherry was stable both in early autophagosomes and autolysosomes (red fluorescence). We also quantified the number of early autophagosomes alone (both red and green fluorescence). As soon as an early autophagosome fuses with a lysosome, the drop in pH quenches GFP fluorescence. The percentage flux was then calculated as the ratio of early autophagosomes over total autolysosomes using the following formula: Flux (%) =  $[(100 - (\text{red and green/red}) \times 100)]$ .

### Western blot analysis

Cells were washed in PBS and then lysed using lysis buffer [1 M Tris, 2.5 M NaCl, 10% glycerol, 0.5 M glycerophosphate, 1% Tween-20, 0.5% Nonidet P-40 and 1× EDTA-free Complete Protease Inhibitor tablet (Roche)] for 15 min on ice. Extracts were separated by SDS-PAGE (on 10% or 12% polyacrylamide gels) and transferred to a nitrocellulose membrane (Whatman). The blots were incubated with the specific antibodies and developed according to the manufacturer's instructions (ECL Prime, Amersham).

### Co-immunoprecipitation assay

Immunoprecipitation of endogenous Atg5–Atg12 and Atg16L1 were performed in HaCaT or in iASPP-expressing HEK293 cells. Cells were lysed in lysis buffer, as described above. Immunoprecipitation was performed by incubating 1 mg of cleared cell lysates with 1 µg of antibody against Atg5–Atg12 or Atg16L1 at 4°C overnight. Protein-G–Sepharose beads (50 µl, GE Healthcare) were added, incubated for 2 h at 4°C, precipitated and washed three times with NP-40 lysis buffer. The immunoprecipitates were subjected to SDS-PAGE, and Atg5–Atg12, Atg16L1 and iASPP were detected by western blot analysis as described above. Quantification of the immunoprecipitates was performed by using the densitometry values. The percentage of Atg5 in complex with Atg16L1 or iASPP was obtained using the following formulae: (1) Percentage of Atg5 bound to iASPP =  $[(\text{Atg5 IP}/\text{Atg5 input})/(\text{iASPP IP}/\text{iASPP input}) \times 100]$  and (2) Percentage of Atg5 bound to Atg16L1 =  $[(\text{Atg5 IP}/\text{Atg5 input})/(\text{Atg16L1 IP}/\text{Atg16L1 input}) \times 100]$ , where IP and input represent the densitometry values of the specific protein in the immunoprecipitate and input, respectively.

### LysoTracker labeling

HaCaT (sh-control and sh-iASPP), N-TERT (sh-control and sh-iASPP), and differentiated cells, were loaded with LysoTracker Red (100 nM, L7528, Invitrogen) and carbocyanine dye DiIC<sub>1</sub>(5) (40 nM, H14700, Invitrogen) by incubating the cells with the dyes for 1 h or 15 min, respectively, at 37°C. Cells were then washed in PBS buffer (D8537, Invitrogen) and resuspended in 400 µl of PBS, in the presence of the DNA-staining viability dye DAPI (200 ng/ml) (D9542, Sigma).

### ROS and annexin V labeling

HaCaT (Sh-control and Sh-iASPP), N-TERT (Sh-control and Sh-iASPP), as well as differentiated cells, were loaded with MitoSox (5 µM, M36008, Invitrogen) by incubating the cells with the dye for 30 min at 37°C. Cells were then washed in PBS buffer and resuspended in 100 µl of Ca<sup>2+</sup>-rich buffer with annexin-V–FITC (2.5 µl) (556547 Becton Dickinson). Cells were then incubated at room temperature for 15 min. The DNA-staining viability dye DAPI (200 ng/ml) was added just before flow cytometric analysis.

### Indirect immunofluorescence LC3B labeling

HaCaT (sh-control and sh-iASPP), N-TERT (sh-control and sh-iASPP) and differentiated cells with or without treatment were pelleted and resuspended in 100 µl of Solution A fixative (GAS-002A-1, Caltag, UK) for 15 min at room temperature. Cells were then washed in PBS buffer and were permeabilized by incubation in 0.25% Triton X-100 for 15 min at room temperature, followed by washing in PBS buffer. Anti-LC3B polyclonal antibody (0.25 µg) (L10382, Invitrogen) or rabbit immunoglobulin (0.25 µg, used as an isotype control) (I5006, Sigma)

was added, and the samples were incubated for 30 min at room temperature. The cells were then washed in PBS buffer and incubated with 0.125 µg of Alexa-Fluor-647-conjugated goat anti-rabbit-IgG (A21244, Invitrogen) for 30 min at room temperature. Cells were then washed in PBS buffer and resuspended in 400 µl of PBS, in the presence of DAPI (200 ng/ml). Analysis of the Alexa-Fluor-647 signal was achieved by determining the median fluorescence intensity (MFI) of the whole histogram signal for previously live cells gated from a forward scatter (FSC) versus side scatter (SSC) dot-plot and compared with the MFI of the corresponding isotype control sample in an overlaid histogram. For each sample, 10,000 events were collected by flow cytometry.

### Flow cytometry

Single color controls for annexin-V–FITC or LysoTracker Red, DiIC<sub>1</sub>(5), MitoSOX and DAPI were used to set compensations. Annexin-V–FITC or LysoTracker Green was detected in the 530/25-nm channel on the argon laser octagon (BD LSR II); MitoSOX was detected on the 610/20-nm channel on the BD LSR II; DiIC<sub>1</sub>(5) was detected in the 660/20-nm channel on Red HeNe trigon (BD LSR II); DAPI was detected in the 440/40-nm channel on the violet diode trigon (BD LSR II). LC3B–Alexa-Fluor-647-labeled cells and DAPI (200 ng/ml) were analyzed in the 660/20 nm channel on Red HeNe trigon (BD LSR II). Cells were analyzed on a Becton Dickinson LSR II fitted with a 488-nm Ti-Sapphire Argon laser, Red HeNe 633-nm diode, UV laser 350–360 nm and violet diode 405 nm. All data were analyzed on BD FACS Diva software (v6.1.3).

### Antibodies

Antibodies against the following proteins were used: from Abcam – KDEL ER marker (mouse monoclonal), GOLGA2/GM130 (cis-Golgi matrix protein, Golgi marker; mouse monoclonal), proteasome 20S protein (rabbit polyclonal) and GAPDH (rabbit monoclonal); from Neomarkers – p63 (clone 4A4, for western blotting); from Santa Cruz (for immunofluorescence) – Bcl-2, Bcl-xL, MFN1, MFN2, p62, Tomm20, ULK1 and p63 (H129 and H137); from Sigma – iASPP (clone LXO49.3) and Atg5; gifts from Irene Leigh – KRT1, KRT14, loricerin, involucrin and Ki67; from Cell Signaling Technologies – pro-caspase 8, pro-caspase 9, Puma, Noxa, Mcl-1, Bim, LC3, Atg16L1, Atg7, Rab9, phospho-S6 ribosomal protein (Ser240/244), S6 ribosomal protein, phospho-4E-BP1 (Ser65), 4E-BP1, cleaved PARP and phospho-mTOR (Ser 2448); from Epitomics – beclin-1; and from Becton Dickinson – DRP1 and OPA1.

### RNA interference

For iASPP knockdown, primary keratinocytes were transfected with a SMARTpool of four siRNAs (Dharmacon, UK) targeting iASPP (L-003815-00-0020). For p63 knockdown, siRNA sequences against p63 (ID 217143, ID 4893 and ID 217144; Applied Biosystems) were used in combination to create an siRNA-p63 pool. For Noxa knockdown, cells were transfected with a SMARTpool of four siRNAs (Dharmacon, UK) targeting Noxa (J-005275). For Atg5 knockdown, four siGENOME siRNAs (D-004374-01, D-004374-03, D-004374-05, D-004374-06) were used in combination (Dharmacon, UK). Transfection was performed according to the manufacturer's protocol and optimized for a six-well plate. Briefly, cells were plated at 50% confluency and subjected to transfection on the following day using 15 µl of HiPerFect (Qiagen, UK) transfection reagent and 60 nM final concentration of each siRNA. Transfection media were replaced with complete DMEM after 24 h. iASPP, p63, Noxa or Atg5 protein expression was analyzed by western blotting at 48 h post-transfection. Cells incubated with the transfection reagent only (control) and cells transfected with a pool of non-targeting siRNAs (siCONTROL non-targeting siRNA pool) were used as negative controls.

### Microarray analysis

Whole Human Genome 4×44K Oligo Microarrays (Agilent Technologies) were used to compare the expression profiles of

keratinocytes with or without iASPP silencing (sh-ctrl versus sh-iASPP). The Agilent protocol used was described previously (Chikh et al., 2011).

### DNA constructs

The plasmid for Noxa overexpression was a generous gift from Alan Storey. The plasmids for beclin1–GFP and LC3–GFP overexpression were generous gifts from Ciro Isidoro. The tandem tagged LC3 (tFLC3) was a generous gift from Tamotsu Yoshimori.

### Acknowledgements

We would like to thank Tania Maffucci (Blizard Institute, London, UK) and Marco Falasca (Blizard Institute, London, UK) for helpful discussions about the manuscript. We are grateful to Tamotsu Yoshimori (Osaka University, Osaka, Japan), Luca Scorrano (Venetian Institute of Molecular Medicine, Padova, Italy), Alan Storey (Oxford University, Oxford, UK), Irene Leigh (Dundee University, Dundee, UK) and Ciro Isidoro (Università degli studi del Piemonte Orientale Amedeo Avogadro, Novara, Italy) for providing constructs and antibodies. We would also like to thank Ann Wheeler (Blizard Institute, London, UK) for assistance with confocal microscopy.

### Competing interests

The authors declare no competing interests.

### Author contributions

A.C. and D.B. planned the experiments; A.C. performed most of the experiments with some contributions from P.S.; G.C., C.R., O.A., G.W., C.B. and C.A.H. provided technical support and intellectual contribution to the project. D.B. wrote the manuscript together with A.C. and C.A.H.

### Funding

Funding support was provided by Barts and The London Charity.

### Supplementary material

Supplementary material available online at <http://jcs.biologists.org/lookup/suppl/doi:10.1242/jcs.144816/-DC1>

### References

- Aymard, E., Barruche, V., Naves, T., Bordes, S., Closs, B., Verdier, M. and Ratinaud, M. H. (2011). Autophagy in human keratinocytes: an early step of the differentiation? *Exp. Dermatol.* **20**, 263–268.
- Baerga, R., Zhang, Y., Chen, P. H., Goldman, S. and Jin, S. (2009). Targeted deletion of autophagy-related 5 (atg5) impairs adipogenesis in a cellular model and in mice. *Autophagy* **5**, 1118–1130.
- Bellot, G. L., Liu, D. and Pervaiz, S. (2013). ROS, autophagy, mitochondria and cancer: Ras, the hidden master? *Mitochondrion* **13**, 155–162.
- Bergamaschi, D., Samuels, Y., O'Neil, N. J., Trigiant, G., Crook, T., Hsieh, J. K., O'Connor, D. J., Zhong, S., Campargue, I., Tomlinson, M. L. et al. (2003). iASPP oncoprotein is a key inhibitor of p53 conserved from worm to human. *Nat. Genet.* **33**, 162–167.
- Bergamaschi, D., Samuels, Y., Sullivan, A., Zvebil, M., Breyssens, H., Bisso, A., Del Sal, G., Syed, N., Smith, P., Gasco, M. et al. (2006). iASPP preferentially binds p53 proline-rich region and modulates apoptotic function of codon 72-polymorphic p53. *Nat. Genet.* **38**, 1133–1141.
- Bonnet, S., Archer, S. L., Allalunis-Turner, J., Haromy, A., Beaulieu, C., Thompson, R., Lee, C. T., Lopaschuk, G. D., Puttagunta, L., Bonnet, S. et al. (2007). A mitochondria-K<sup>+</sup> channel axis is suppressed in cancer and its normalization promotes apoptosis and inhibits cancer growth. *Cancer Cell* **11**, 37–51.
- Cai, Y., Qiu, S., Gao, X., Gu, S. Z. and Liu, Z. J. (2012). iASPP inhibits p53-independent apoptosis by inhibiting transcriptional activity of p63/p73 on promoters of proapoptotic genes. *Apoptosis* **17**, 777–783.
- Candi, E., Schmidt, R. and Melino, G. (2005). The cornified envelope: a model of cell death in the skin. *Nat. Rev. Mol. Cell Biol.* **6**, 328–340.
- Cao, L., Huang, Q., He, J., Lu, J. and Xiong, Y. (2013). Elevated expression of iASPP correlates with poor prognosis and chemoresistance/radioresistance in FIGO Ib1–IIa squamous cell cervical cancer. *Cell Tissue Res.* **352**, 361–369.
- Chang, T. K., Shravage, B. V., Hayes, S. D., Powers, C. M., Simin, R. T., Wade Harper, J. and Baehrecke, E. H. (2013). Uba1 functions in Atg7- and Atg3-independent autophagy. *Nat. Cell Biol.* **15**, 1067–1078.
- Chatterjea, S. M., Resing, K. A., Old, W., Nirunskiri, W. and Fleckman, P. (2011). Optimization of flagrin expression and processing in cultured rat keratinocytes. *J. Dermatol. Sci.* **61**, 51–59.
- Chen, H. and Chan, D. C. (2009). Mitochondrial dynamics – fusion, fission, movement, and mitophagy – in neurodegenerative diseases. *Hum. Mol. Genet.* **18** R2, R169–R176.
- Chen, J., Xie, F., Zhang, L. and Jiang, W. G. (2010). iASPP is over-expressed in human non-small cell lung cancer and regulates the proliferation of lung cancer cells through a p53 associated pathway. *BMC Cancer* **10**, 694.
- Chikh, A., Matin, R. N., Senatore, V., Huffbauer, M., Lavery, D., Raimondi, C., Ostano, P., Mello-Grand, M., Ghimentì, C., Bahta, A. et al. (2011). iASPP/p63 autoregulatory feedback loop is required for the homeostasis of stratified epithelia. *EMBO J.* **30**, 4261–4273.
- Chikte, S., Panchal, N. and Warnes, G. (2014). Use of LysoTracker dyes: A flow cytometric study of autophagy. *Cytometry A* **85**, 169–178.
- Chipuk, J. E. and Green, D. R. (2008). How do BCL-2 proteins induce mitochondrial outer membrane permeabilization? *Trends Cell Biol.* **18**, 157–164.
- Ciechomska, I. A., Goemans, G. C., Skepper, J. N. and Tolkovsky, A. M. (2009). Bcl-2 complexed with Beclin-1 maintains full anti-apoptotic function. *Oncogene* **28**, 2128–2141.
- Claerhout, S., Dutta, B., Bossuyt, W., Zhang, F., Nguyen-Charles, C., Dennison, J. B., Yu, Q., Yu, S., Balázi, G., Lu, Y. et al. (2012). Abortive autophagy induces endoplasmic reticulum stress and cell death in cancer cells. *PLoS ONE* **7**, e39400.
- Collins, T. J., Berridge, M. J., Lipp, P. and Bootman, M. D. (2002). Mitochondria are morphologically and functionally heterogeneous within cells. *EMBO J.* **21**, 1616–1627.
- Deruy, E., Gosselin, K., Vercamer, C., Martien, S., Bouali, F., Slomianny, C., Bertout, J., Bernard, D., Pourtier, A. and Abbadie, C. (2010). MnSOD upregulation induces autophagic programmed cell death in senescent keratinocytes. *PLoS ONE* **5**, e12712.
- Fuchs, E. (1990). Epidermal differentiation: the bare essentials. *J. Cell Biol.* **111**, 2807–2814.
- Germain, M., Nguyen, A. P., Le Grand, J. N., Arbour, N., Vanderluit, J. L., Park, D. S., Opferman, J. T. and Slack, R. S. (2011). MCL-1 is a stress sensor that regulates autophagy in a developmentally regulated manner. *EMBO J.* **30**, 395–407.
- Gomes, L. C. and Scorrano, L. (2013). Mitochondrial morphology in mitophagy and macroautophagy. *Biochim. Biophys. Acta* **1833**, 205–212.
- Gosselin, K., Deruy, E., Martien, S., Vercamer, C., Bouali, F., Dujardin, T., Slomianny, C., Houel-Renault, L., Chelli, F., De Launoit, Y. et al. (2009). Senescent keratinocytes die by autophagic programmed cell death. *Am. J. Pathol.* **174**, 423–435.
- Griffiths, R. E., Kupzig, S., Cogan, N., Mankelov, T. J., Betin, V. M., Trakarsanga, K., Massey, E. J., Parsons, S. F., Anstee, D. J. and Lane, J. D. (2012). The ins and outs of human reticulocyte maturation: autophagy and the endosome/exosome pathway. *Autophagy* **8**, 1150–1151.
- Herron, B. J., Rao, C., Liu, S., Laprade, L., Richardson, J. A., Olivieri, E., Semsarian, C., Millar, S. E., Stubbs, L. and Beier, D. R. (2005). A mutation in NFκB interacting protein 1 results in cardiomyopathy and abnormal skin development in wa3 mice. *Hum. Genet.* **14**, 667–677.
- Jiang, L., Siu, M. K., Wong, O. G., Tam, K. F., Lu, X., Lam, E. W., Ngan, H. Y., Le, X. F., Wong, E. S., Monteiro, L. J. et al. (2011). iASPP and chemoresistance in ovarian cancers: effects on paclitaxel-mediated mitotic catastrophe. *Clin. Cancer Res.* **17**, 6924–6933.
- Kabeya, Y., Mizushima, N., Ueno, T., Yamamoto, A., Kirisako, T., Noda, T., Kominami, E., Ohsumi, Y. and Yoshimori, T. (2000). LC3, a mammalian homologue of yeast Apg8p, is localized in autophagosomes after processing. *EMBO J.* **19**, 5720–5728.
- Kim, R., Emi, M., Tanabe, K. and Murakami, S. (2006). Role of the unfolded protein response in cell death. *Apoptosis* **11**, 5–13.
- Kimura, S., Noda, T. and Yoshimori, T. (2007). Dissection of the autophagosome maturation process by a novel reporter protein, tandem fluorescent-tagged LC3. *Autophagy* **3**, 452–460.
- Klionsky, D. J. (2009). Autophagy in mammalian systems, Part B. Preface. *Methods Enzymol.* **452**, xxi–xxii.
- Laska, M. J., Strandbygd, D., Kjeldgaard, A., Mains, M., Corydon, T. J., Memon, A. A., Sørensen, B. S., Vogel, U., Jensen, U. B. and Nexø, B. A. (2007). Expression of the RAI gene is conducive to apoptosis: studies of induction and interference. *Exp. Cell Res.* **313**, 2611–2621.
- Lee, H. M., Shin, D. M., Yuk, J. M., Shi, G., Choi, D. K., Lee, S. H., Huang, S. M., Kim, J. M., Kim, C. D., Lee, J. H. et al. (2011). Autophagy negatively regulates keratinocyte inflammatory responses via scaffolding protein p62/SQSTM1. *J. Immunol.* **186**, 1248–1258.
- Lee, J., Giordano, S. and Zhang, J. (2012). Autophagy, mitochondria and oxidative stress: cross-talk and redox signalling. *Biochem. J.* **441**, 523–540.
- Li, G., Wang, R., Gao, J., Deng, K., Wei, J. and Wei, Y. (2011). RNA interference-mediated silencing of iASPP induces cell proliferation inhibition and G0/G1 cell cycle arrest in U251 human glioblastoma cells. *Mol. Cell. Biochem.* **350**, 193–200.
- Li, S., Shi, G., Yuan, H., Zhou, T., Zhang, Q., Zhu, H. and Wang, X. (2012). Abnormal expression pattern of the ASPP family of proteins in human non-small cell lung cancer and regulatory functions on apoptosis through p53 by iASPP. *Oncol. Rep.* **28**, 133–140.
- Liu, Z. J., Cai, Y., Hou, L., Gao, X., Xin, H. M., Lu, X., Zhong, S., Gu, S. Z. and Chen, J. (2008). Effect of RNA interference of iASPP on the apoptosis in MCF-7 breast cancer cells. *Cancer Invest.* **26**, 878–882.
- Liu, H., Wang, M., Diao, S., Rao, Q., Zhang, X., Xing, H. and Wang, J. (2009). siRNA-mediated down-regulation of iASPP promotes apoptosis induced by etoposide and daunorubicin in leukemia cells expressing wild-type p53. *Leuk. Res.* **33**, 1243–1248.
- Liu, Z., Zhang, X., Huang, D., Liu, Y., Zhang, X., Liu, L., Li, G., Dai, Y., Tan, H., Xiao, J. et al. (2012). Elevated expression of iASPP in head and neck squamous cell carcinoma and its clinical significance. *Med. Oncol.* **29**, 3381–3388.
- Lowman, X. H., McDonnell, M. A., Kosloske, A., Odumade, O. A., Jenness, C., Karim, C. B., Jemmerson, R. and Kelekar, A. (2010). The proapoptotic

- function of Noxa in human leukemia cells is regulated by the kinase Cdk5 and by glucose. *Mol. Cell* **40**, 823–833.
- Lu, B., Guo, H., Zhao, J., Wang, C., Wu, G., Pang, M., Tong, X., Bu, F., Liang, A., Hou, S. et al. (2010). Increased expression of iASPP, regulated by hepatitis B virus X protein-mediated NF-kappaB activation, in hepatocellular carcinoma. *Gastroenterology* **139**, 2183–2194 e2185.
- Lum, J. J., Bauer, D. E., Kong, M., Harris, M. H., Li, C., Lindsten, T. and Thompson, C. B. (2005). Growth factor regulation of autophagy and cell survival in the absence of apoptosis. *Cell* **120**, 237–248.
- Maiuri, M. C., Ciriollo, A., Tasdemir, E., Vicencio, J. M., Tajeddine, N., Hickman, J. A., Geneste, O. and Kroemer, G. (2007). BH3-only proteins and BH3 mimetics induce autophagy by competitively disrupting the interaction between Beclin 1 and Bcl-2/Bcl-X(L). *Autophagy* **3**, 374–376.
- Mantovani, F., Tocco, F., Girardini, J., Smith, P., Gasco, M., Lu, X., Crook, T. and Del Sal, G. (2007). The prolyl isomerase Pin1 orchestrates p53 acetylation and dissociation from the apoptosis inhibitor iASPP. *Nat. Struct. Mol. Biol.* **14**, 912–920.
- Milani, M., Rzymiski, T., Mellor, H. R., Pike, L., Bottini, A., Generali, D. and Harris, A. L. (2009). The role of ATF4 stabilization and autophagy in resistance of breast cancer cells treated with Bortezomib. *Cancer Res.* **69**, 4415–4423.
- Mizushima, N., Yamamoto, A., Hatano, M., Kobayashi, Y., Kabeya, Y., Suzuki, K., Tokuhiwa, T., Ohsumi, Y. and Yoshimori, T. (2001). Dissection of autophagosome formation using Apg5-deficient mouse embryonic stem cells. *J. Cell Biol.* **152**, 657–668.
- Mizushima, N., Kuma, A., Kobayashi, Y., Yamamoto, A., Matsubae, M., Takao, T., Natsume, T., Ohsumi, Y. and Yoshimori, T. (2003). Mouse Apg16L, a novel WD-repeat protein, targets to the autophagic isolation membrane with the Apg12-Apg5 conjugate. *J. Cell Sci.* **116**, 1679–1688.
- Mizushima, N., Yoshimori, T. and Levine, B. (2010). Methods in mammalian autophagy research. *Cell* **140**, 313–326.
- Mizushima, N., Yoshimori, T. and Ohsumi, Y. (2011). The role of Atg proteins in autophagosome formation. *Annu. Rev. Cell Dev. Biol.* **27**, 107–132.
- Naik, E., Michalak, E. M., Villunger, A., Adams, J. M. and Strasser, A. (2007). Ultraviolet radiation triggers apoptosis of fibroblasts and skin keratinocytes mainly via the BH3-only protein Noxa. *J. Cell Biol.* **176**, 415–424.
- Nishida, Y., Arakawa, S., Fujitani, K., Yamaguchi, H., Mizuta, T., Kanaseki, T., Komatsu, M., Otsu, K., Tsujimoto, Y. and Shimizu, S. (2009). Discovery of Atg5/Atg7-independent alternative macroautophagy. *Nature* **461**, 654–658.
- Notari, M., Hu, Y., Koch, S., Lu, M., Ratnayaka, I., Zhong, S., Baer, C., Pagotto, A., Goldin, R., Salter, V. et al. (2011). Inhibitor of apoptosis-stimulating protein of p53 (iASPP) prevents senescence and is required for epithelial stratification. *Proc. Natl. Acad. Sci. USA* **108**, 16645–16650.
- Nyfeler, B., Bergman, P., Wilson, C. J. and Murphy, L. O. (2012). Quantitative visualization of autophagy induction by mTOR inhibitors. *Methods Mol. Biol.* **821**, 239–250.
- Nys, K., Van Laethem, A., Michiels, C., Rubio, N., Piette, J. G., Garmyn, M. and Agostinis, P. (2010). A p38(MAPK)/HIF-1 pathway initiated by UVB irradiation is required to induce Noxa and apoptosis of human keratinocytes. *J. Invest. Dermatol.* **130**, 2269–2276.
- Paglin, S., Lee, N. Y., Nakar, C., Fitzgerald, M., Plotkin, J., Deuel, B., Hackett, N., McMahon, M., Sphicas, E., Lampen, N. et al. (2005). Rapamycin-sensitive pathway regulates mitochondrial membrane potential, autophagy, and survival in irradiated MCF-7 cells. *Cancer Res.* **65**, 11061–11070.
- Pang, M. S., Chen, X., Lu, B., Zhao, J., Li, B. H., Wei, Y. Q. and Guo, Y. J. (2010). Lentiviral vector-mediated doxycycline-inducible iASPP gene targeted RNA interference in hepatocellular carcinoma. *Chin J. Cancer* **29**, 796–801.
- Pyo, J. O., Yoo, S. M., Ahn, H. H., Nah, J., Hong, S. H., Kam, T. I., Jung, S. and Jung, Y. K. (2013). Overexpression of Atg5 in mice activates autophagy and extends lifespan. *Nat. Commun.* **4**, 2300.
- Ravikumar, B. and Rubinsztein, D. C. (2006). Role of autophagy in the clearance of mutant huntingtin: a step towards therapy? *Mol. Aspects Med.* **27**, 520–527.
- Rossiter, H., König, U., Barresi, C., Buchberger, M., Ghannadan, M., Zhang, C. F., Mlitz, V., Gmeiner, R., Sukserree, S., Födinger, D. et al. (2013). Epidermal keratinocytes form a functional skin barrier in the absence of Atg7 dependent autophagy. *J. Dermatol. Sci.* **71**, 67–75.
- Sæbø, M., Skjelbred, C. F., Nexø, B. A., Wallin, H., Hansteen, I. L., Vogel, U. and Kure, E. H. (2006). Increased mRNA expression levels of ERCC1, OGG1 and RAI in colorectal adenomas and carcinomas. *BMC Cancer* **6**, 208.
- Salemi, S., Yousefi, S., Constantinescu, M. A., Fey, M. F. and Simon, H. U. (2012). Autophagy is required for self-renewal and differentiation of adult human stem cells. *Cell Res.* **22**, 432–435.
- Shimizu, S., Arakawa, S. and Nishida, Y. (2010). Autophagy takes an alternative pathway. *Autophagy* **6**, 290–291.
- Silva, J. N., Galmiche, A., Tomé, J. P., Boullier, A., Neves, M. G., Silva, E. M., Capiod, J. C., Cavaleiro, J. A., Santus, R., Mazière, J. C. et al. (2010). Chain-dependent photocytotoxicity of tricationic porphyrin conjugates and related mechanisms of cell death in proliferating human skin keratinocytes. *Biochem. Pharmacol.* **80**, 1373–1385.
- Simpson, M. A., Cook, R. W., Solanki, P., Patton, M. A., Dennis, J. A. and Crosby, A. H. (2009). A mutation in NF-kappaB interacting protein 1 causes cardiomyopathy and woolly haircoat syndrome of Poll Hereford cattle. *Anim. Genet.* **40**, 42–46.
- Sugiura, K., Muro, Y., Futamura, K., Matsumoto, K., Hashimoto, N., Nishizawa, Y., Nagasaka, T., Saito, H., Tomita, Y. and Usukura, J. (2009). The unfolded protein response is activated in differentiating epidermal keratinocytes. *J. Invest. Dermatol.* **129**, 2126–2135.
- Sukserree, S., Rossiter, H., Mildner, M., Pammer, J., Buchberger, M., Gruber, F., Watanapokasin, R., Tschachler, E. and Eckhart, L. (2013). Targeted deletion of Atg5 reveals differential roles of autophagy in keratin K5-expressing epithelia. *Biochem. Biophys. Res. Commun. Commun.* **430**, 689–694.
- Sultana, H., Kigawa, J., Kanamori, Y., Itamochi, H., Oishi, T., Sato, S., Kamazawa, S., Ohwada, M., Suzuki, M. and Terakawa, N. (2003). Chemoresponsiveness and p53-Bax pathway-mediated apoptosis in patients with uterine cervical cancer. *Ann. Oncol.* **14**, 214–219.
- Tait, S. W. and Green, D. R. (2010). Mitochondria and cell death: outer membrane permeabilization and beyond. *Nat. Rev. Mol. Cell Biol.* **11**, 621–632.
- Tamiji, S., Beauvillain, J. C., Mortier, L., Jouy, N., Tual, M., Delaporte, E., Formstecher, P., Marchetti, P. and Polakowska, R. (2005). Induction of apoptosis-like mitochondrial impairment triggers antioxidant and Bcl-2-dependent keratinocyte differentiation. *J. Invest. Dermatol.* **125**, 647–658.
- Tong, X., Smith, K. A. and Pelling, J. C. (2012). Apigenin, a chemopreventive bioflavonoid, induces AMP-activated protein kinase activation in human keratinocytes. *Mol. Carcinog.* **51**, 268–279.
- Toonen, J., Liang, L. and Sidjanin, D. J. (2012). Waved with open eyelids 2 (woe2) is a novel spontaneous mouse mutation in the protein phosphatase 1, regulatory (inhibitor) subunit 13 like (Ppp1r13l) gene. *BMC Genet.* **13**, 76.
- Tormo, D., Checińska, A., Alonso-Curbelo, D., Pérez-Guijarro, E., Cañón, E., Riveiro-Falkenbach, E., Calvo, T. G., Larrubere, L., Megías, D., Mulero, F. et al. (2009). Targeted activation of innate immunity for therapeutic induction of autophagy and apoptosis in melanoma cells. *Cancer Cell* **16**, 103–114.
- Trigiante, G. and Lu, X. (2006). ASPP [corrected] and cancer. *Nat. Rev. Cancer* **6**, 217–226.
- Villunger, A., Michalak, E. M., Coultas, L., Müllauer, F., Böck, G., Ausserlechner, M. J., Adams, J. M. and Strasser, A. (2003). p53- and drug-induced apoptotic responses mediated by BH3-only proteins puma and noxa. *Science* **302**, 1036–1038.
- Wang, R. C. and Levine, B. (2011). Calcipotriol induces autophagy in HeLa cells and keratinocytes. *J. Invest. Dermatol.* **131**, 990–993.
- Wang, Y., Wang, X. D., Lapi, E., Sullivan, A., Jia, W., He, Y. W., Ratnayaka, I., Zhong, S., Goldin, R. D., Goemans, C. G. et al. (2012). Autophagic activity dictates the cellular response to oncogenic RAS. *Proc. Natl. Acad. Sci. USA* **109**, 13325–13330.
- Watt, F. M. (1989). Terminal differentiation of epidermal keratinocytes. *Curr. Opin. Cell Biol.* **1**, 1107–1115.
- Zhang, X., Wang, M., Zhou, C., Chen, S. and Wang, J. (2005). The expression of iASPP in acute leukemias. *Leuk. Res.* **29**, 179–183.
- Zhang, B., Xiao, H. J., Chen, J., Tao, X. and Cai, L. H. (2011). Inhibitory member of the apoptosis-stimulating protein of p53 (ASPP) family promotes growth and tumorigenesis in human p53-deficient prostate cancer cells. *Prostate Cancer Prostatic Dis.* **14**, 219–224.
- Zhao, J., Brault, J. J., Schild, A., Cao, P., Sandri, M., Schiaffino, S., Lecker, S. H. and Goldberg, A. L. (2007). FoxO3 coordinately activates protein degradation by the autophagic/lysosomal and proteasomal pathways in atrophying muscle cells. *Cell Metab.* **6**, 472–483.
- Zhao, Y., Howe, J. L., Yu, Z., Leong, D. T., Chu, J. J., Loo, J. S. and Ng, K. W. (2013). Exposure to titanium dioxide nanoparticles induces autophagy in primary human keratinocytes. *Small* **9**, 387–392.
- Zhou, X. and Münger, K. (2009). Expression of the human papillomavirus type 16 E7 oncoprotein induces an autophagy-related process and sensitizes normal human keratinocytes to cell death in response to growth factor deprivation. *Virology* **385**, 192–197.